Biosensors and Bioelectronics 90 (2017) 418–435

Contents lists available at ScienceDirect

Biosensors and Bioelectronics

journal homepage: www.elsevier.com/locate/bios

Magnetic impedance biosensor: A review

Tao Wang[a], Yong Zhou[b], Chong Lei[b], Jun Luo[a], Shaorong Xie[a], Huayan Pu[a,*]

[a] School of Mechatronics Engineering and Automation, Shanghai University, Shanghai 200072, China
[b] Key Laboratory for Thin Film and Microfabrication of Ministry of Education, Department of Micro/Nano Electronics, School of electronic information and electrical engineering, Shanghai Jiao Tong University, Shanghai 200240, China

ARTICLE INFO

Keywords:
Magnetoimpedance biosensor
Detection
Magnetic nanoparticles
Label
Cancer cell
Biomolecule

ABSTRACT

Though the magnetoimpedance effect was discovered two decades ago, the biomedical applications of the magnetoimpedance sensor are still in their infancy. In this review, the authors summarized the magnetoimpedance effect in soft ferromagnetic wires, ribbons and thin films for biosensing applications. Recent progress and achievements of the magnetoimpedance-based biosensing applications including the detection of magnetic Ferrofluid, magnetic beads, magnetic nanoparticles, magnetically labeled bioanalytes and biomagnetic fields of living systems were reviewed. The modification effect of the biochemical liquids, agglomeration effect of the magnetic particles, and the effect of the stray magnetic field on magnetoimpedance were investigated in this review. Some constructive strategies were proposed for design of the high-performance magnetoimpedance biosensor, for quantitative and ultrasensitive detection of magnetically labeled biomolecules. The theoretical and experimental results suggest that the magnetoimpedance sensors are particularly suitable for highly sensitive detection of low-concentration biomolecules, and might be used for early diagnosis and screening of cancers.

1. Introduction

Superparamagnetic particles such as magnetic beads (< 100 μm) and magnetic nanoparticles (< 100 nm) are of great interest for researchers from a wide range of the disciplines (Drozdov et al., 2016; Fuentes et al., 2005; Huang et al., 2015; Jahanbani et al., 2016; Liang et al., 2012; Palecek et al., 2007; Paul et al., 2012; Pflipsen et al., 2013; Sun et al., 2008; Uddin et al., 2016) because of their unique physical and chemical properties, including magnetic fluids, catalysis, magnetic resonance imaging, data storage, environmental remediation, biotechnology and bioengineering. magnetic particles are commonly composed of magnetic elements, such as iron, nickel, cobalt and their oxides. Superparamagnetic particles can be magnetized only if subjected to an external magnetic field, so no residual magnetization retains in the absence of magnetic field. They are also easily functionalized with different biochemical substances that can be used to capture deoxyribonucleic acid, protein, enzymes and cells. Physicochemical stability of the superparamagnetic particles enables the detection and magnetic manipulation both in vitro and in vivo, without affecting the biological interactions. Functionalized superparamagnetic particles are widely used for *biomedical* applications such as immunoassay (Rong et al., 2016), magnetic resonance imaging (Bi et al., 2015), telomerase activity (Zhou et al., 2008), nucleic acid isolation (Berensmeier, 2006) and magnetic separation (Yavuz et al., 2006) due to their easy-to-functionalization, superparamagnetism, physicochemical stability and biocompatibility.

Living systems can produce biomagnetic fields because they are electrically excitable. Magnetic sensors with sufficiently high sensitivity are able to detect the biomagnetic fields produced by the biologic tissues or organs, thus providing a non-invasive mean to detect the activity of the living systems.

The investigation of magnetic biosensor can be traced back to 1998. Baselt et al. (1998) used a magnetoresistive sensor to detect the presence of micron-sized magnetic particles which can be used as bimolecular labels. Since then, Resonant coil sensor (Lu et al., 2006; Richardson et al., 2001; Stevenson et al., 2005), Fluxgate sensor (Heim et al., 2009; Ludwig et al., 2005a, 2005b), Hall sensor (Besse et al., 2002; Ejsing et al., 2004; Østerberg et al., 2013; Lee et al., 2009; Manzin et al., 2012; Sandhu et al., 2007; Sinha et al., 2014), Tunnel magnetoresistive sensor (Albon et al., 2009; Li et al., 2014; Shen et al., 2005), Giant magnetoresistance sensor (Albisetti et al., 2013; Choi et al., 2016; De Boer et al., 2007; Gaster et al., 2009; Hall et al., 2010; Koets et al., 2009; Lee et al., 2014; Manteca et al., 2011; Mujika et al., 2009; Ng et al., 2016; Miller et al., 2001; Oh et al., 2013; Pannetier et al., 2011; Rife et al., 2003; Shoshi et al., 2013; Srinivasan et al., 2009), Spin valve sensor (Ferreira et al., 2002; Graham et al., 2002,

* Corresponding author.
E-mail address: phygood_2001@shu.edu.cn (H. Pu).

http://dx.doi.org/10.1016/j.bios.2016.10.031
Received 29 July 2016; Received in revised form 12 October 2016; Accepted 18 October 2016
Available online 20 October 2016
0956-5663/

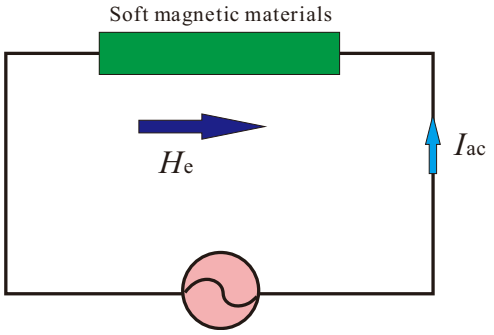

Fig. 1. The GMI effect in the soft magnetic materials.

2003; Martins et al., 2009; Serrate et al., 2012), anisotropic magnetoresistance sensor (Jiang et al., 2006; Miller et al., 2002; Rizzi et al., 2014) and Superconducting quantum interference (Drung et al., 2007; Hao et al., 2011; Matz et al., 1999) were proposed as a biosensor for biomagnetic detections. Recently, giant magnetoimpedance (GMI) effect has attracted *much* attention because of its potential application in magnetic field sensing. The GMI effect (Beach and Berkowitz, 1994; Knobel et al., 2002; Panina et al., 1994, 1995; Phan et al., 2008) is considered as a large variation of the complex impedance of the soft magnetic materials carrying an alternating current (AC) upon the application of an external magnetic field (H_e), as shown in Fig. 1. When the external magnetic field was applied along the longitudinal direction of the soft magnetic materials, we call it longitudinal GMI effect. When the external magnetic field was applied along the transverse direction of the soft magnetic materials, we call it transverse GMI effect. When the external magnetic field was applied perpendicularly to the direction of materials thickness, we call it perpendicular GMI effect. So far, much attention has been focused on longitudinal GMI effect due to its many advantages in sensor applications. The GMI effect can be characterized by the relative ratio of the impedance, GMI ratio or MI ratio ($\Delta Z/Z$), see Eq. (1). The impedance can be expressed by Eq. (2), thus, the change in AC giant magnetoresistance (GMR) and giant magnetoreactance (GMX) with the applied field at a given frequency of the driving current can be defined as the GMR ratio or MR ratio ($\Delta R/R$) and GMX ratio or MX ratio ($\Delta X/X$) according to Eqs. (3) and (4), respectively. The GMI effect can be understood in terms of the combination of high-frequency skin effect (Jackson, 1975; Landau and Lifshitz, 1975; Wheeler, 1942) of AC and a strong field dependence of the magnetic permeability associated with a particular magnetic domain structure (Beach and Berkowitz, 1994; Knobel et al., 2002; Panina et al., 1994, 1995; Phan et al., 2008) in soft magnetic materials. Skin effect is the tendency of an AC to become distributed within a conductor such that the current density is largest near the surface of the conductor, and decreases with greater depths in the conductor. The penetrate depth below the conductor surface in which the AC falls on the surface is called as the skin depth (Jackson, 1975; Landau and Lifshitz, 1975; Wheeler, 1942). The skin effect causes the effective resistance of the conductor to increase at higher frequencies where the skin depth is smaller, thus resulting in the high-frequency GMI effect. It was reported that the magnetic-field sensitivity of GMI in quenched wires (Vazquez et al., 2001), quenched ribbons (Phan et al., 2006) and multilayer films (Morikawa et al., 1996) can reach an extremely large value of several hundred%/Oe at high frequency (>1 MHz). Consequently, the GMI effect is very useful for development of highly sensitive magnetic sensors. Furthermore, it is possible to develop GMI-based biosensors for detection of the magnetic beads, the magnetic nanoparticles, the magnetic labeled bioanalytes, even the biomagnetic fields of the living systems.

$$\text{GMI ratio} = \Delta Z/Z = 100\% \times \frac{Z(H) - Z(H_{max})}{Z(H_{max})} \quad (1)$$

$$Z = R + jX \quad (2)$$

$$\text{GMR ratio} = \Delta R/R = 100\% \times \frac{R(H) - R(H_{max})}{R(H_{max})} \quad (3)$$

$$\text{GMX ratio} = \Delta X/X = 100\% \times \frac{X(H) - X(H_{max})}{X(H_{max})} \quad (4)$$

2. Detection of magnetic particles

2.1. Detection of magnetic Ferrofluid

The GMI sensor was introduced into the field of biosensors by Kurlyandskaya et al. (2003). They reported a GMI biosensor prototype based on a commercial Vitrovac® CoFeMoSiB ribbon (1×0.02×100 mm) for detection of Ferrofluid, which opens the gate for GMI-based biosensing applications. Magnetoimpedance was measured by the four-point technique, two of which were used for exciting current contacts. The other two Cu-leads were used for measuring contacts. During the testing, Ferrofluid® (10 nm) was spread uniformly on the ribbon in a direct-contact way, a bias magnetic field (± 150 Oe) was applied by using a pair of Helmholtz coils parallel to the ribbon axis, and a sinusoidal drive current (0.3–10 MHz) flowed through the sample along the longitudinal ribbon axis, see Fig. 2(a) (Kurlyandskaya et al., 2003). Superparamagnetic beads became strongly magnetized in the presence of H_e and the transverse AC magnetic field, thus causing the beads to produce a stray magnetic field, thereby modifying superimposed magnetic fields and then altering the magnetoimpedance of the sensing elements.

Experimental results [Fig. 2(b)] show that the GMI response is greatly enhanced at high frequency (1–10 MHz) in the presence of Ferrofluid. Although the detection sensitivity may be improved by testing the particles on the ribbon in a direct-contact way, the biochemical fluids such as acid can contaminate and even damage the GMI sensitive elements in the biosensing experiments. Theoretically speaking, the no-contact testing is probably a better way to detect the magnetic particles. In addition, they observed an interesting phenomenon: *the GMI effect enhances (< 6 Oe) first and* then drops (> 6 Oe) due to the presence of magnetic Ferrofluid, as shown in Fig. 2(c). Unfortunately, theoretical explanations for this phenomenon are absent.

In 2014, a GMI sensor based on $[FeNi/Cu]_4/FeNi/Cu/[FeNi/Cu]_4FeNi$ films has been used to detect the spherical iron particles (500 μm) and the ferrofluids containing iron oxide nanoparticles (Yuvchenko et al., 2014). Basically, the more the spherical iron particles, the stronger the stray magnetic fields, and the larger changes the impedance. It is worthwhile to note that the presence of the ferrofluid residue (4% concentration) on the surface of the sensor has caused a drop (Fig. 3) in GMI effect (Yuvchenko et al., 2014), which is completely different from the previous results (Kurlyandskaya et al., 2003). This will be discussed in subsequent chapters.

Recently, Kurlyandskaya et al. (2012) reported an electroplated CuBe/FeCoNi wire for detection of magnetic ferrofluid. They observed that the presence of ferrofluid led to a significant reduction of the GMI ratio and an increase of the high-field hysteresis of GMI. However, Amirabadizadeh et al. (2016) studied the GMI effect in a CoFeSiB amorphous wire surrounded by the magnetite ferrofluid. They observed that the GMI effect was greatly enhanced due to the presence of magnetite ferrofluid on the sensor. In the presence of ferrofluid, the maximum GMI ratio increases from 315% to 417% and also the sensitivity increases about 150% at frequency of 4.5 MHz. There is no appreciable difference between the two testing methods. This is most likely due to the different superimposed magnetic fields induced by different ferrofluid distributions.

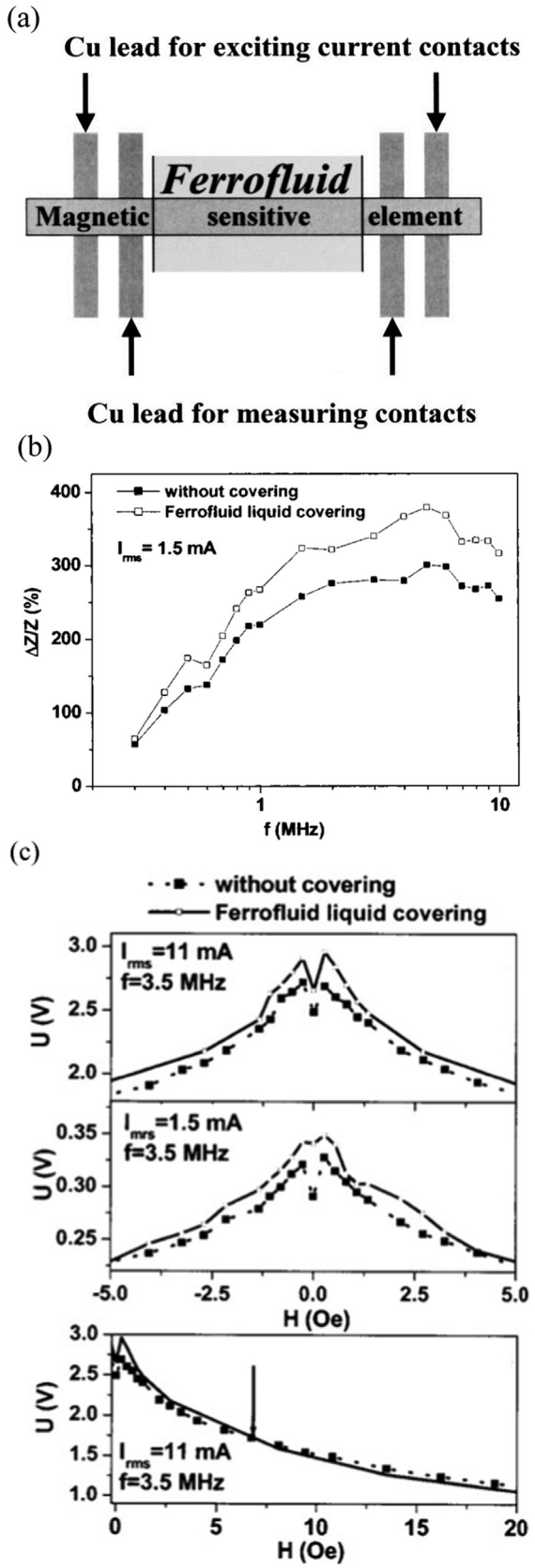

Fig. 2. (a) Scheme of testing the Ferrofluid using a GMI sensor; (b) Frequency and (c) Field dependence of the MI response of uncovered and Ferrofluid-covered sensitive element (Kurlyandskaya et al., 2003).

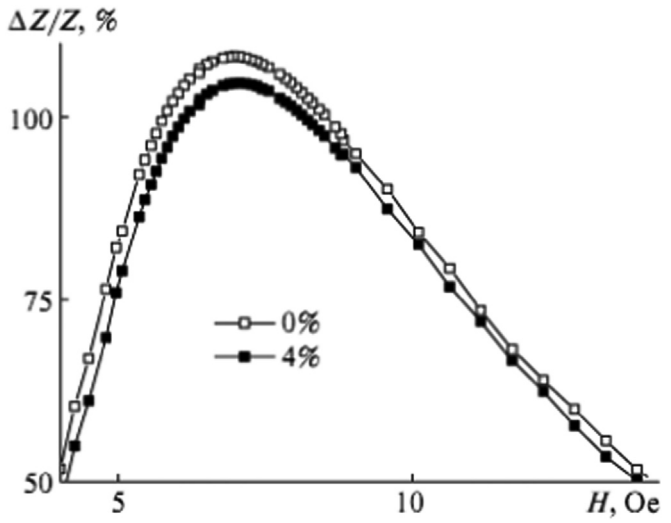

Fig. 3. Relative change in MI versus the magnetic field strength in the absence and in the presence of the ferrofluid residue (4%) on the surface of the meander (Yuvchenko et al., 2014).

2.2. Detection of magnetic beads

2.2.1. Detection of Dynabeads® M-450 using a CoFeMoSiB ribbon

In order to explore the possibilities of using GMI sensor for magnetic beads-labeled bioassay, a GMI sensor based on an amorphous CoFeMoSiB ribbon was used to detect Dynabeads® M-450 (4.5 μm) (Kurlyandskaya et al., 2005). In the experiments, the GMI responses of two samples were measured by standard four point technique, one of which was the ribbon with phosphate buffered saline (PBS) containing the Dynabeads, another was only the ribbon with PBS. Experimental results (Kurlyandskaya et al., 2005) show there is a clear difference in the GMI responses between the samples with and without Dynabeads, and the presence of Dynabeads causes a significant enhancement in GMI effect. It's worth noting that Kurlyandskaya et al. (2005) also used the direct-contact testing method to detect the Dynabeads in this study.

2.2.2. Detection of Dynabeads® M-480 using sandwiched films

In 2008, Kurlyandskaya (2009) detected the Dynabeads® M-480 (8.8×106, 4.4×107 beads/ml) using a GMI sensor based on sandwiched films (NiFe/Cu/NiFe), the results are shown in Fig. 4. As can be seen from Fig. 4(a) and (b), the GMI response enhances (> −6 Oe) firstly and then drops (< −6 Oe), which is in accordance with the results reported in previous study (Kurlyandskaya et al., 2003). As the curve shifts due to the presence of particles, we call it offset GMI effect.

It's worth noting that Kurlyandskaya (2009) have fabricated a GMI sensor consisting of a ribbon sandwiched between two Au films. The good biocompatibility of the Au films makes the GMI sensor possible for biosensing applications. However, the skin effect of AC current flowing through the ribbon was greatly undermined because the Au films (non-magnetic) became the major paths of AC due to their high conductivity. Thus, the GMI effect was greatly reduced, as shown in Fig. 4(c) (Kurlyandskaya, 2009). The low GMI effect may result in low sensitivity in detecting weak magnetic field. Alternatively, in order to protect and maintain good performance of the GMI sensor, an insulating layer is needed to insert between the Au film and the soft magnetic layers.

2.2.3. Detection of magnetite microparticles and Dynabeads® M-450 under continuous flow

Most of the past GMI-based biosensing researches focus on detecting the presence of magnetic microparticles in a static regime, which largely restricts the biosensing applications of the GMI sensor

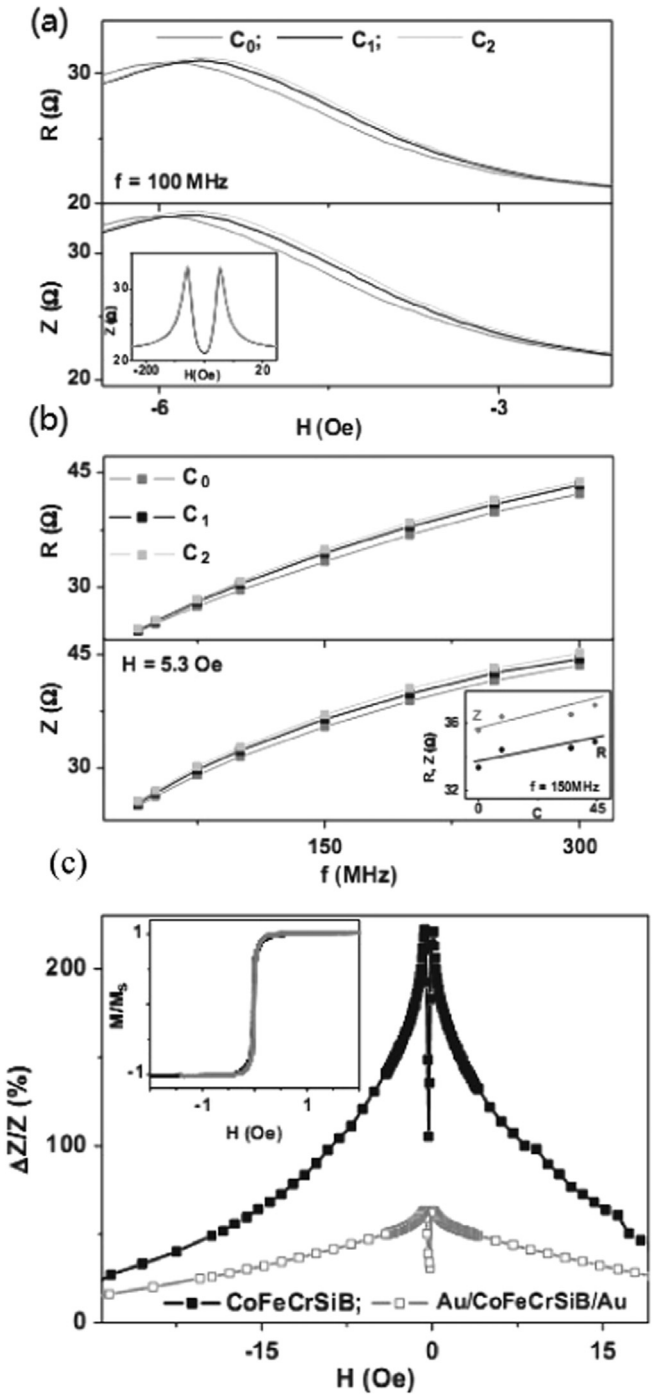

Fig. 4. GMI responses of FeNi/Cu/FeNi element in presence of Dynabeads M-480® (C0=0, C1=8.8×10^6, C2=4.4×10^7 (beads/ml)) (a) Field dependency and (b) Frequency dependency; (c) GMI responses of the CoFeCrSiB ribbon and the Au-coated CoFeCrSiB ribbon (Kurlyandskaya, 2009).

since many bioassaies need to be performed in a dynamic state such as liquid chromatogram, polymerase chain reaction, electrophoresis and magnetophoresis analysis etc. Recently, Kurlyandskaya et al. (García-Arribas et al., 2011) designed a microfluidic GMI sensor for detection of the magnetic beads under continuous flow of the carrier fluid, which lays a solid foundation for development of GMI-based lab-on-chip device. This microfluidic sensor was comprised of a 10 μm chamber with two channels situated on top of the soft magnetic materials. It was capable of detecting the presence of magnetic particles in continuous flow (García-Arribas et al., 2011), as shown in Fig. 5.

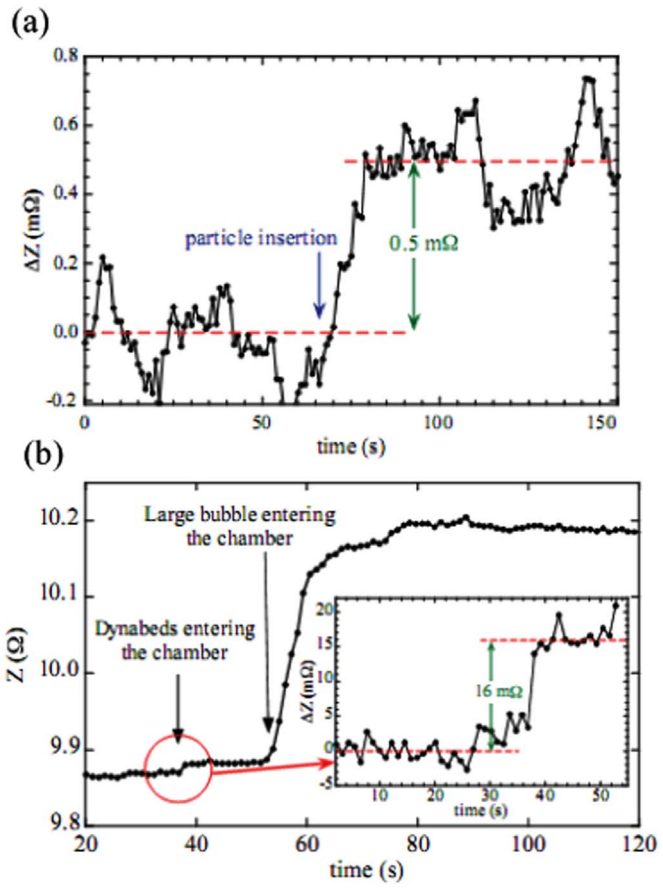

Fig. 5. Impedance changes of a GMI sensor in the presence of PBS with Dynabeads in continuous flow (a) amorphous ribbon (b) multilayer films (García-Arribas et al., 2011).

2.2.4. Detection of Co microparticles and Estapor beads

In 2005, a wire-based GMI biosensor in combination with the magnetic labeling technique for detecting biomolecules was proposed by Chiriac et al. (2005), the detection scheme is shown in Fig. 6(a). In this scheme, a polymer layer was coated on the sensing element for capturing the target biomolecules such as deoxyribonucleic acid (DNA). Subsequently, the target biomolecules were hybridized with tagged molecule such as biotin. Thereafter, the magnetic particles functionalized with specific bioprobe such as avidin were introduced to mark DNA through the biotin-avidin bond. Hence, detection of DNA can be realized by probing the magnetic dipole fields of the magnetized magnetic particles using the GMI sensor. The proposed scheme provides theoretic guidance for development of GMI sensor in magnetic immunoassay. Significantly, Chiriac et al. proposed that the magnetic particles could be detected by the microwire under a perpendicular magnetic field. In our view, the microwire is not suitable for on-chip (in-situ) magnetic labeling detection owing to its circular structure. However, the on-chip (in-situ) magnetic labeling detection using perpendicular magnetizing method may be particularly applicable to films or ribbons because the magnetic particles can be distributed uniformly on the films or ribbons in the presence of the perpendicular magnetic field (Kurlyandskaya and Levit, 2007). This magnetizing method will be discussed in more detail at a later stage. During the detection of Co magnetic microparticles, Chiriac et al. (2005) observed that the impedance response of the CoFeSiB amorphous microwire remained stable when the particles exceeded 2000, as shown in Fig. 6(b). Later in 2007, Chiriac et al. (Chiriac et al., 2007) used a GMI sensor formed by several CoFeSiB amorphous microwires to detect the Estapor beads (1.9 μm). They found that the presence of beads caused a decline in magnetoimpedance, and the detection sensitivity increased with increasing the number of microwire, as

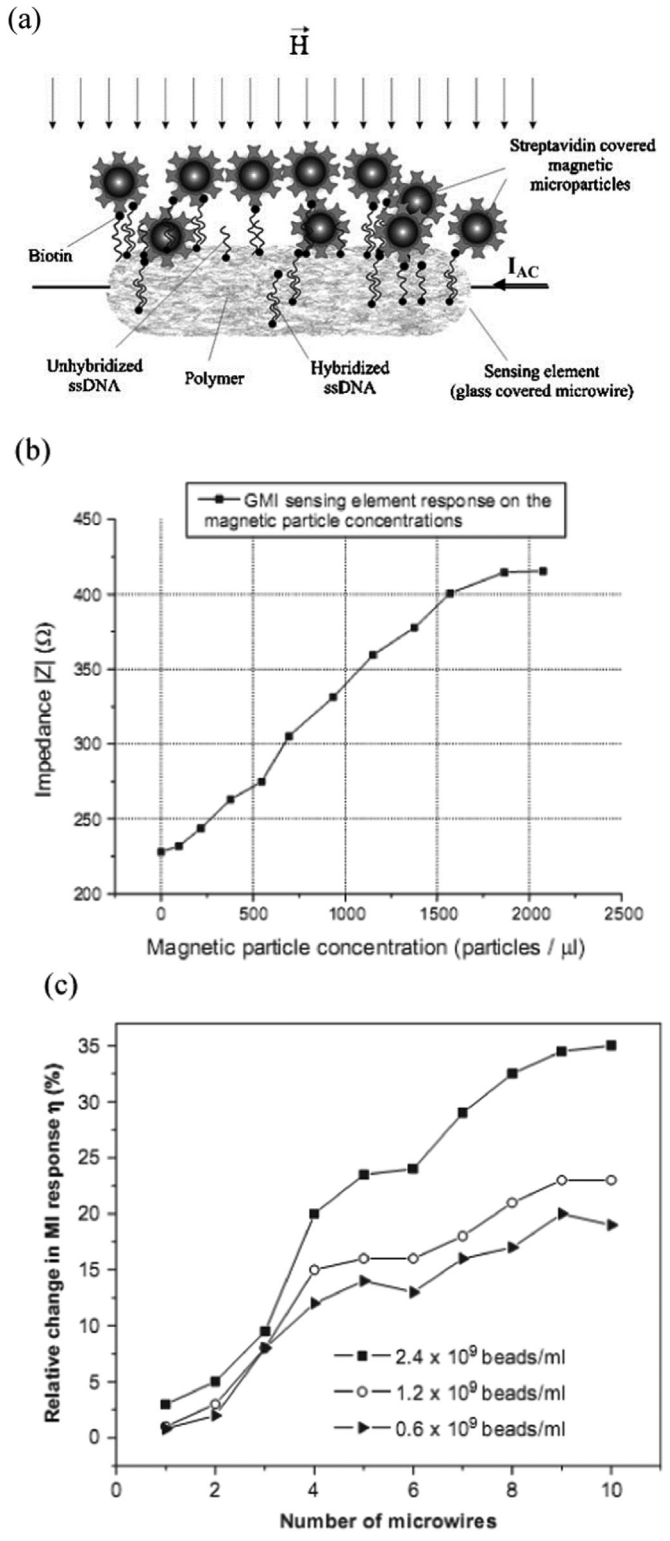

Fig. 6. (a) Schematic diagram of using the GMI biosensor to detect DNA; (b) The relationship between the impedance response and the magnetic particle concentrations; (c) Relative change in MI response of different microwire arrays for different bead concentrations (Chiriac et al., 2005, 2007).

shown in Fig. 6(c) (Chiriac et al., 2007). Hence, it is possible to fabricate high-sensitive GMI biosensor based on microwires through integrating multiple microwires.

2.2.5. Quantitative detection of Dynabeads® Protein A using multilayered films

There are two major issues in the previous GMI-based particle detections: One is that the early studies focus on qualitative or half-quantitative level, but there have been few studies reporting on quantitative detection of magnetic beads by using GMI sensors. The other is that the direct-contact testing method was used in most of the previous GMI-based particle detections. Recently, we adopted two non-contact testing methods (Wang et al., 2013a, 2014a) for quantification of magnetic beads: separated-type testing method and in-situ testing method, as shown in Fig. 7(a) and (b).

In 2013, we fabricated a GMI biosensor based on multilayered films (Cr/Cu/NiFe/Cu/NiFe/Al_2O_3/Cr/Au) for biosensing applications. In this structure, NiFe/Cu/NiFe films were used as the sensitive elements, Au film was used for immobilization of magnetic beads, and Al_2O_3 film was used as an insulating layer for protecting the sensitive elements from contamination. We used a separated-type testing method *based on the GMI biosensor for quan*titative analysis of magnetic beads (Wang et al., 2013a). During the experiments, Dynabeads® protein A (2.8 μm) were immobilized on a quadrate Au film other than on the sensitive element, then the Au film was placed near the sensor (Cr/Cu/NiFe/Cu/NiFe/Al_2O_3/Cr/Au) for testing, as shown in Fig. 7(a) (Wang et al., 2013a). After applying a constant longitudinal external magnetic field (0–125 Oe), the superparamagnetic Dynabeads were magnetized longitudinally near the sensor, and the intrinsic magnetic moments of Dynabeads should be uniformly rotated to the longitudinal direction. The magnetic moments give rise to a small stray magnetic field that influences the GMI. It was found that the GMI effect was reduced in the presence of Dynabeads, as shown in Figs. 7(c) and 7(d) (Wang et al., 2013a). This *differs from* some reported results (Kurlyandskaya et al., 2005; Kurlyandskaya et al., 2003) where the presence of magnetic particles has caused an enhanced GMI effect. Kurlyandskaya et al. observed a similar phenomenon lately, the presence of ferrofluid residue (4% concentration) on the sensor also resulted in a drop of GMI (Yuvchenko et al., 2014). *Quan*titative detection of low-concentration Dynabeads® protein A (0.1–5 μg/ml) was realized by using the separated-type testing method, as shown in Fig. 7(e). This method is simple, fast in running and easy to use, which lays the foundation for quantitative analysis of bioanalytes.

We also have developed a non-contact in-situ testing method of combining the GMI biosensor based on multilayered films (Cr/Cu/NiFe/Cu/NiFe/Al_2O_3/Cr/Au) for quantitative determination of the magnetic beads, as shown in Fig. 7(b) (Wang et al., 2014a). Quantification of low-concentration Dynabeads® protein A (0.1–10 μg/ml) was achieved by using the GMI biosensor, as shown in Figs. 7(f), 7(g) and 7(h) (Wang et al., 2014a).

It's worth noting that high detection sensitivities for magnetic particles are often obtained near the maximum GMI ratio, as seen in Fig. 7 (Wang et al., 2013a, 2014a). This is attributed to not only the large stray magnetic fields induced by the strong external magnetic field, but also the high field-sensitivities obtained at the anisotropy field. The transverse permeability reaches the maximum at the anisotropy field as a result of the large contribution from rotational magnetization (Panina et al., 1995). The GMI response of the beads becomes smaller at higher external magnetic field (> 30 Oe). This is because the stray magnetic fields may be strongly overwhelmed by the overlarge external magnetic field. There is no obvious changes in GMI ratio at low external magnetic field (< 10 Oe), which can be explained by the low-level magnetization of the magnetic particles and the magnetic hysteresis in GMI sensor at low external magnetic field.

As can be seen from Fig. 7 (Wang et al., 2013a, 2014a), the high detection sensitivities are obtained at medium frequency (several MHz). This is because the GMI sensor is highly sensitive to the external magnetic field at medium frequency since domain wall displacement and spin rotation both contribute to the transverse permeability, thus leading to the high detection sensitivities at medium frequency (Panina

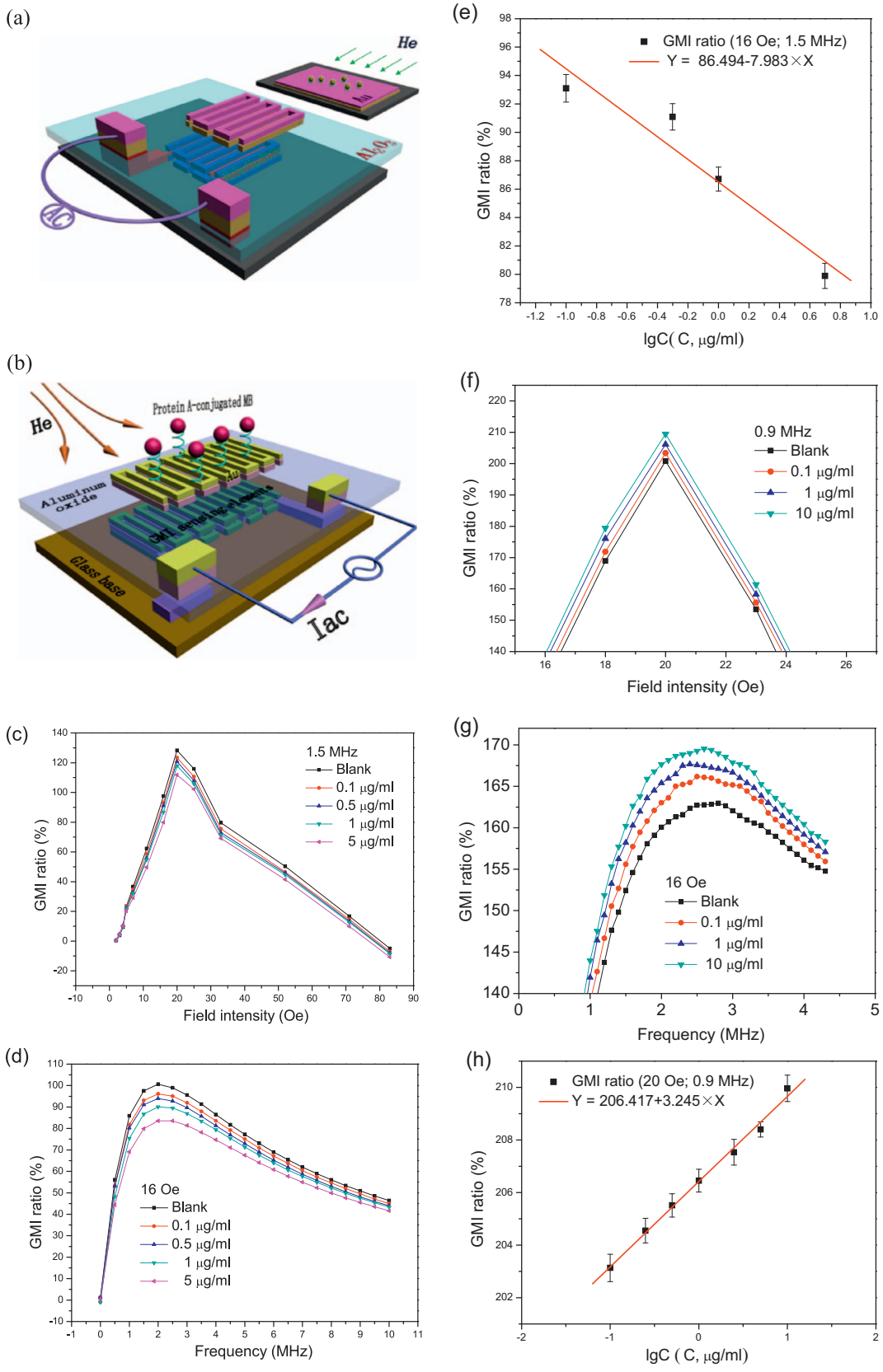

Fig. 7. (a) The GMI-based separated-type testing method for detecting Dynabeads® Protein A; (b) The GMI-based in-situ testing method for detecting Dynabeads® Protein A; (c) Field dependence of GMI responses of detecting the Dynabeads® protein A (separated-type); (d) Frequency dependence of GMI responses of detecting the Dynabeads® protein A (separated-type); (e) the linear relationship between the concentration of Dynabeads® Protein A and GMI response (separated-type); (f) Field dependence of GMI responses of detecting the Dynabeads® protein A (in-situ testing method); (g) Frequency dependence of GMI responses of detecting the Dynabeads® protein A (in-situ); (h) the linear relationship between the concentration of Dynabeads® Protein A and GMI response (in-situ) (Wang et al., 2013a, 2014a).

et al., 1995). As the frequency is further increased (> 5 MHz), domain wall displacement becomes strongly damped, only the spin rotation mechanism contributes to the effective permeability, the GMI effect is thus rather weak, and resulting in low detection sensitivities. At low frequency (< 1 MHz), the skin effect of AC is rather weak, and the field-sensitivities of GMI sensor are very low, thus resulting in low detection sensitivities. Due to the good biocompatibility of the Au film, this GMI biosensor is very promising for in-situ detection of biomolecules through magnetic labeling them on the Au film of the biosensor.

2.2.6. Detection of Dynabeads® MyOne™ Streptavidin C1 and Dynabead® M-280 Streptavidin

Lately, a Co-based GMI sensor with a multilayer structure was adopted for detecting the Dynabeads® MyOne™ Streptavidin C1 and Dynabead® M-280 Streptavidin by Zhou et al. (Yang et al., 2015a). This GMI sensor consists of SiO_2/ribbon/polyimide/SiO_2/Cr/Au films. The SiO_2 layer was used as an insulating layer for protecting the ribbon from contamination. Detection of Dynabeads with various concentrations (1–100 μg/ml) was performed on the GMI sensor. The detection limit for Dynabeads (2.8 μm) can be as low as 700 Dynabeads. This Au-coated GMI sensor based on an amorphous ribbon can be also used as a magnetic biosensor for in-situ detection of biomolecule.

2.3. Detection of magnetic nanoparticles

2.3.1. Detection of Nanomag-D beads using an acid-treated ribbon

Phan et al. introduced an acid-treated ribbon to detect the Nanomag-D beads (Devkota et al., 2013a). It was found that the detection sensitivity of the acid-treated ribbon was *higher than that of* the plain ribbon, as seen in Fig. 8 (Devkota et al., 2013a), which is probably related to the effect of the microholes-pattern produced by the acid on the surface of ribbon. This study provides a new method to improve the sensitivity of GMI sensor in biosensing applications.

2.3.2. MI, MR and MX sensors for detection of Fe_3O_4 nanoparticles

In 2013, Phan et al. adopted a method of combining the MR, MX, and MI effects in an amorphous 2714 A ribbon to detect Fe_3O_4 nanoparticles (Devkota et al., 2013b). Differing from the direct-contact testing methods in previous studies (Kurlyandskaya et al., 2005, 2003, Chiriac et al., 2007), Phan et al. used a non-contact testing method to detect the presence of Fe_3O_4 nanoparticles, namely, a thin parafilm paper was coated on the ribbon to load the nanoparticles in order to protect the sensitive element during the testing. It was found that the MX sensor showed the higher sensitivity than the MR and MI sensors, as shown in Fig. 9 (Devkota et al., 2013b). Therefore, the MX effect is very useful for *development of highly sensitive* magnetic *biosensors*. It's worth noting that the MR, MX and MI responses remain almost unchanged for high particle concentrations (> 124 nM), see Fig. 9(d) (Devkota et al., 2013b), thus, the MR, MX and MI sensors seem more promising for detection of low-concentration superparamagnetic nanoparticles.

2.3.3. Meander-multilayer films for detection of Ni nanoparticles

Recently, Kurlyandskaya et al. reported a GMI sensor based on meander-multilayer films $[FeNi/Cu]_4/FeNi/Cu/[FeNi/Cu]_4/FeNi$ for detection of Ni nanoparticles (Lodewijk et al., 2014). It was found that the GMI sensor was not able to quantify the Ni nanoparticles, and the GMI response was not linear with the particle concentration, as seen in Fig. 10 (Lodewijk et al., 2014).

2.3.4. Multilayer films for detection of ferrogel

Recently, $[FeNi/Ti]_3/Cu/[Ti/FeNi]_3/Ti$ sensitive elements are employed for detection of ferrogels synthesized by radical polymerization of acrylamide in a stable aqueous suspension of r-Fe_2O_3 magnetic nanoparticles (Kurlyandskaya et al., 2015). Ferrogel is a multicomponent system that consists of MNPs dispersed in an elastic cross-linked polymeric net-work swollen in water. Ferrogel falls within the range of the typical values for Young modulus of biological tissues, which makes it an adequate model for the tissues with absorbed magnetic nanoparticles. Precise measurements of the stray magnetic fields of magnetic nanoparticles were realized using either total impedance or its real part variation, which can be used for evaluating the model properties of natural tissues (Kurlyandskaya et al., 2015). Impedance (Z), its real part (R), and imaginary part (X) of the GMI sensor with and without the ferrogels were measured in the frequency range of $1 < f < 600$ MHz. It was found that $\Delta Z/Z$ and $\Delta R/R$ had similar sensitivity of 50%/Oe, nevertheless, the field interval was higher in the $\Delta Z/Z$, as shown in Fig. 11 (Kurlyandskaya et al., 2015).

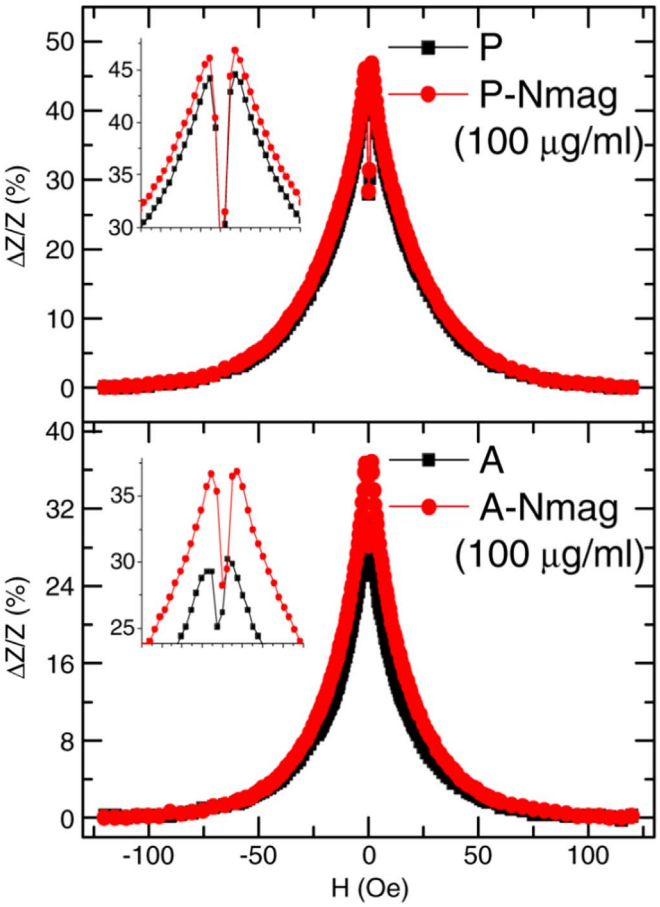

Fig. 8. Magnetic field dependence of magnetoimpedance in untreated ribbon with nanoparticles (P-Nmag) and without nanoparticles (P), acid-treated ribbon with nanoparticles (A-Nmag) and without nanoparticles (A) (Devkota et al., 2013a).

2.3.5. A mathematical model and a microfluidic microsystem for detecting nanoparticles

There have been many reports on experimental studies on the detection of magnetic particles based on the GMI effect, but, as yet, there is lack of accurate theoretical analysis on the GMI-based particle detection. Recently, Senez et al. proposed a mathematical model (Denoual et al., 2011; Fodil et al., 2013, 2014, 2016a, 2016b) for calculating the nanoparticles' magnetic induction induced by a perpendicular magnetic field. The nanoparticles' magnetic induction component along the sensitive axis of the GMI sensor was simulated with different plug lengths, different distances between the sensor and the microchannel, and the time-dependent simulations were also presented. X-direction and Y-direction magnetic induction of the magnetic particles were also theoretically analyzed. It was found that the maximum of X-direction magnetic induction was twice higher than the one of Y-direction magnetic induction. In the experiments, the

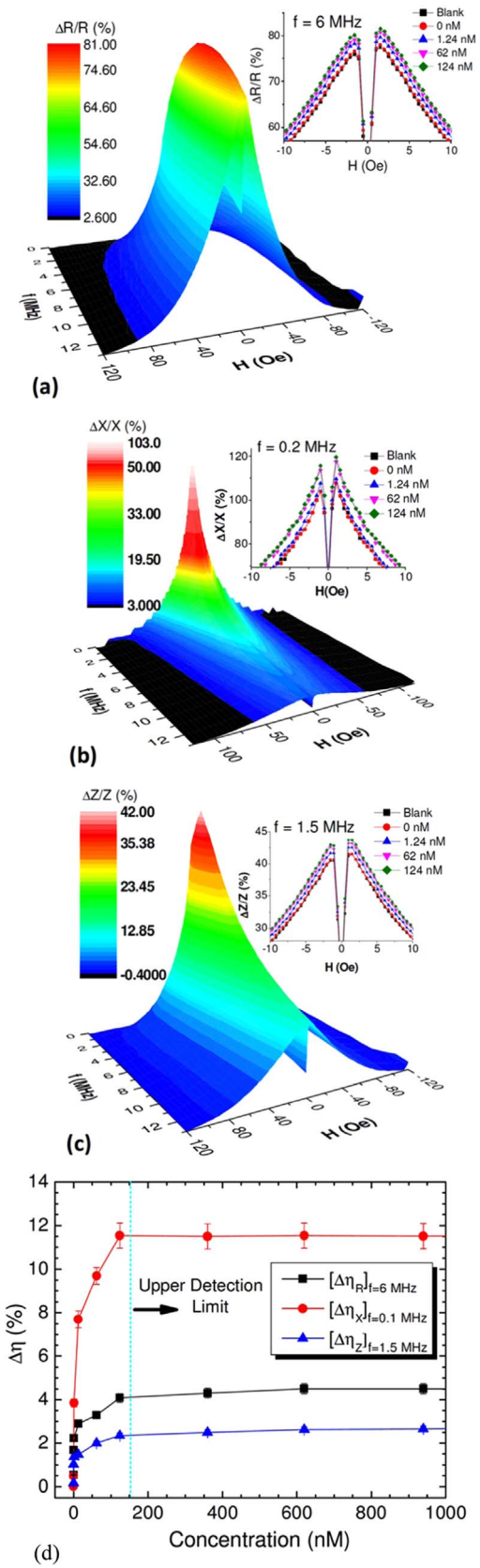

Fig. 9. Magnetic field and frequency dependences of MR (a), MX (b), and MI (c) Ratios for detection of different concentrations of Fe_3O_4 nanoparticles; (d) Relative particle concentration dependence of MR, MX, and MI for detection of the nanoparticles (Devkota et al., 2013b).

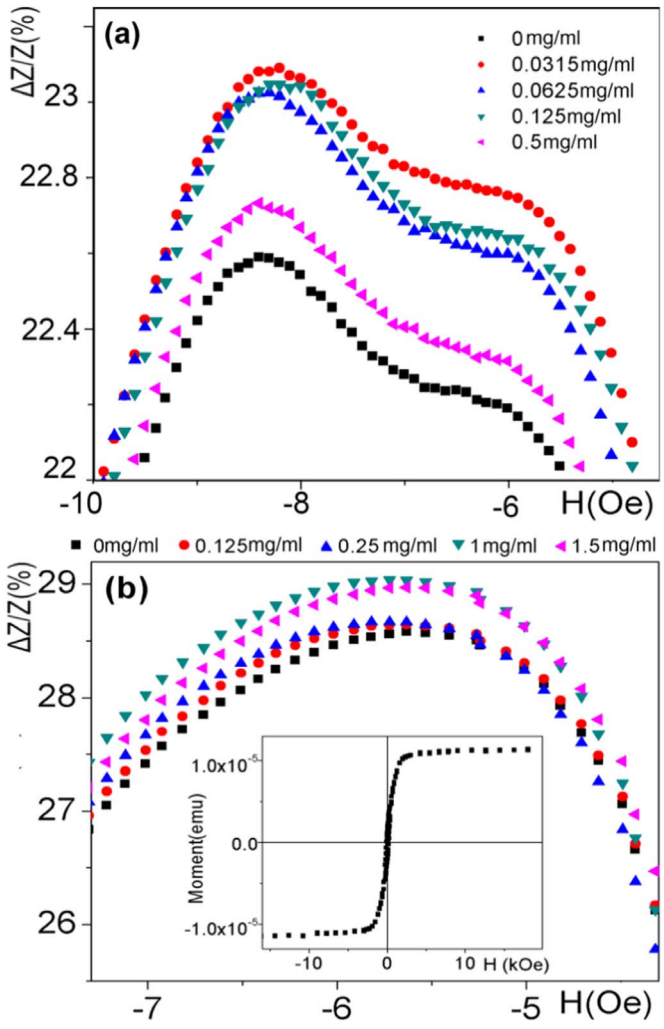

Fig. 10. Magnetic field dependence of GMI ratio for detection of different concentration of Ni nanoparticles (a) Sensor 1 and (b) Sensor 2 (Lodewijk et al., 2014).

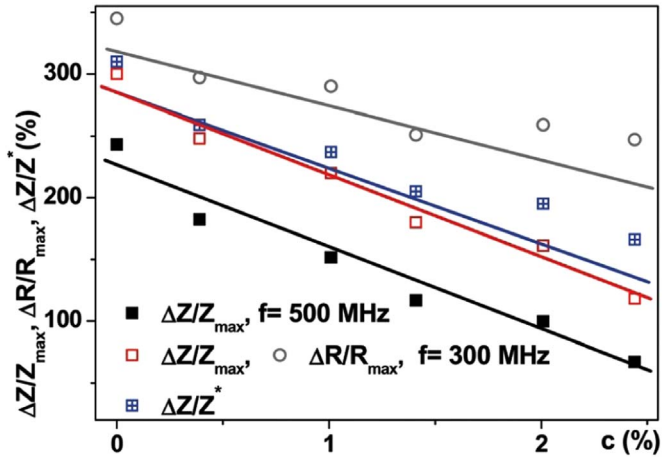

Fig. 11. Field dependences of impedance and its real and imaginary parts of [FeNi/Ti]3/Cu/[Ti/FeNi]3/Ti sensitive element (inset shows GMI and GMR ratios) (Kurlyandskaya et al., 2015).

magnetic nanoparticles were magnetized perpendicularly to the sensitive axis of the sensor and the microchannel in order to obtain better response in detecting the particles, sensitive static and dynamic detection of the magnetic nanoparticles were both achieved *by* means of detecting their stray magnetic fields using a microfluidic channel

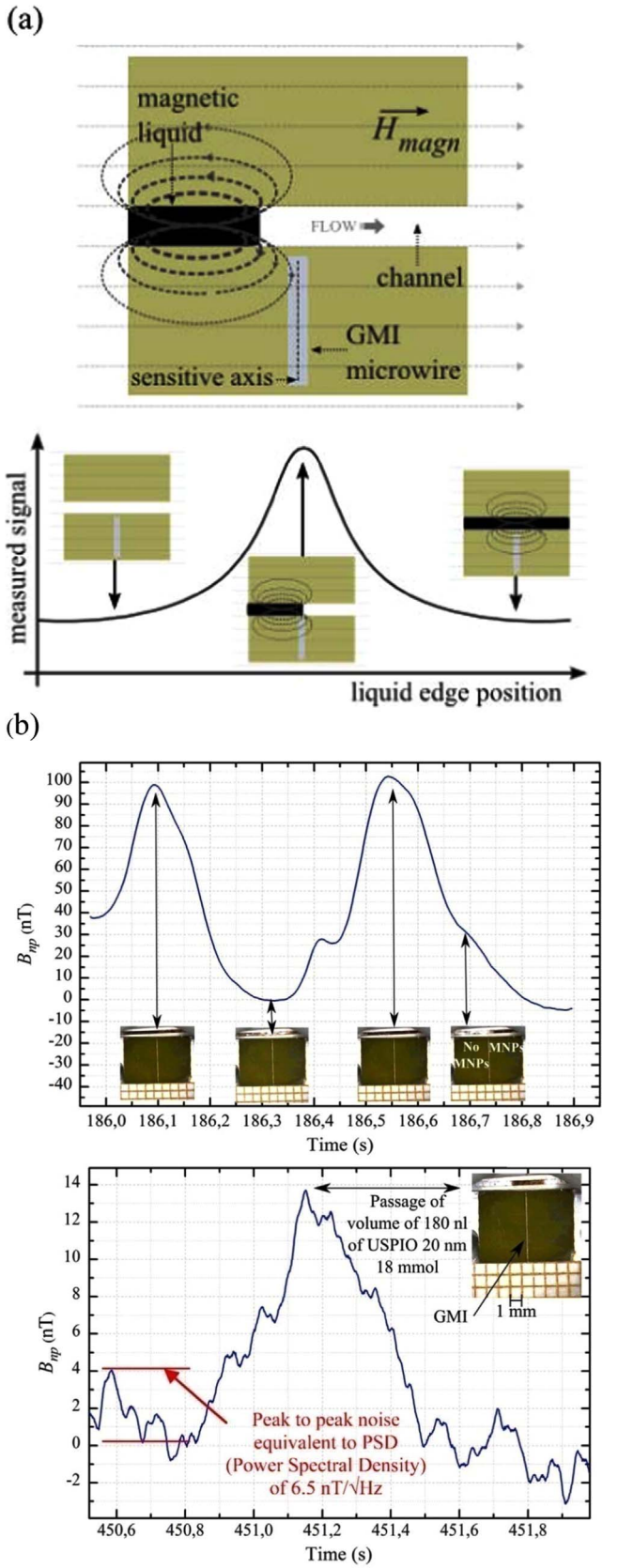

Fig. 12. (a) Schematic view of the general setup for detection of magnetic particles in a microchannel under a perpendicular AC magnetic field; (b) Measured magnetic field during the passage of a given volumes of the nanoparticles in the microchannel (Denoual et al., 2011; Fodil et al., 2013, 2014, 2016a).

involving a microwire-based GMI sensor. The good agreement between theoretical calculations and experimental measurements (Fodil et al., 2014) implies the possibility of using this model to optimize the biosensing system for detecting magnetic nanoparticles.

Senez et al. also developed a microfluidic microsystem integrating a GMI sensor based on a microwire for detection of the magnetic nanoparticles in liquid medium (Denoual et al., 2011; Fodil et al., 2013, 2014, 2016a, 2016b). Differing from the previous works (Devkota et al., 2013b; Kurlyandskaya et al., 2005; Kurlyandskaya et al., 2003; Wang et al., 2013a), they used a perpendicular AC magnetic field to magnetize the magnetic nanoparticles along the microchannel in order to obtain high dynamic range measurements and prevent the saturation of the wire-based GMI sensor, see Fig. 12(a) (Denoual et al., 2011). It was shown that the microfluidic microsystem was capable of detecting the passage of magnetic nanoparticles in liquid medium, see Fig. 12(b) (Fodil et al., 2013), so it has great potential application in flow-dynamic-state biologic microanalyses involving DNA hybridization, polymerase chain reaction reactions, electrophoresis and magnetophoresis analysis etc. Lately, detection of the superparamagnetic iron oxide (20 nm) nanoparticles has been carried out using a GMI-based microsystem. The minimum detectable concentration was as small as 5.47×10^{-9} mol. This research towards a proof of using the GMI sensor combined with superparamagnetic nanoparticles for in-vivo and ex-vivo bio-fluids analyses.

2.4. The agglomeration effect of magnetic particles on GMI

In another our previous work (Wang et al., 2013b), the separated-type testing method was also used to detect Dynabeads in the concentration range of 0.1–100 μg/ml. It has been observed that the GMI response of Dynabeads is not proportional to the Dynabeads' concentration, as seen in Fig. 13(a) and (b) (Wang et al., 2013b), the largest GMI signal is obtained at the lowest concentration (0.1 μg/ml). In this case, we did not disperse the liquid droplet containing the magnetic beads after dropping them on Au film, thus resulting in a cluster of magnetic beads on Au film even at low particle concentration (Wang et al., 2013b). We suggested that the adjacent exciting fields of the Dynabeads had cancelled each other out due to their high-intensity clusters. A similar phenomenon can be seen in Fig. 13(c) and (d) (Wang et al., 2014b), the maximum GMI response of Dynabeads is obtained at a low concentration of 0.1 μg/ml. As can be seen from the Fig. 13, the magnetic beads are unequally distributed at 1 μg/ml, and then start to cluster above 1 μg/ml (Wang et al., 2014b). This is believed to be caused by both inhomogeneous distribution and high-density cluster of Dynabeads. Similar results were also reported by Kurlyandskaya et al. (Lodewijk et al., 2014), Chiriac et al. (2005) and Phan et al. (Devkota et al., 2013b).

Similar results have also been reported in giant magnetoresistive-based biosensing applications (Rife et al., 2003), as shown in Fig. 14. Rife et al. (2003) suggested that the opposing dipole fields of the adjacent beads would reduce the average induced field as the bead density increased, thus the resultant giant magnetoresistive signals became weaker in the presence of high-density magnetic beads (above 1000 beads). They have calculated the stray magnetic field for 2.8 μm bead in a hexagonal array, it was showed that the stray magnetic field was reduced by 9% for adjacent beads separated by a gap of 2.8 μm (1156 beads), and by 23% when the gap was reduced to 1 μm (2530 beads). Martins et al. (2008) also observed a similar phenomenon when the particle concentration exceeds certain value.

To detect high-concentration magnetic beads by using the GMI sensor, there are two main issues that need to be resolved. Firstly, the magnetic beads should be distributed uniformly on the testing platform to avoid the offset effect of stray magnetic fields. It was reported (Kurlyandskaya and Levit, 2007) that the perpendicular magnetic field could induce an ordered self-assembling process of beads and make them distribute uniformly on the fixed platform. Therefore, the

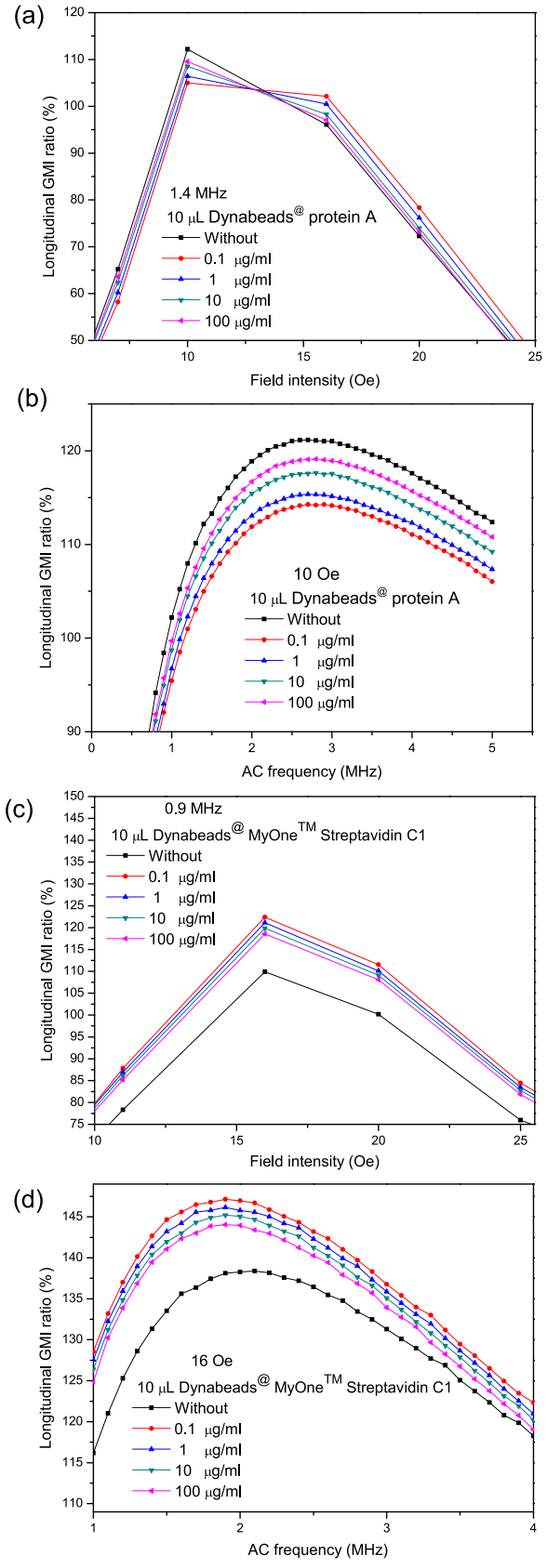

Fig. 13. (a) Field dependence of GMI responses of different-concentration Dynabeads® protein A, (b) Frequency dependence of different-concentration Dynabeads® protein A; (c)Field dependence of GMI responses of different-concentration Dynabeads® MyOne™ Streptavidin C1, (d) Frequency dependence of different-concentration Dynabeads® MyOne™ Streptavidin C1 (Wang et al., 2013b, 2014b).

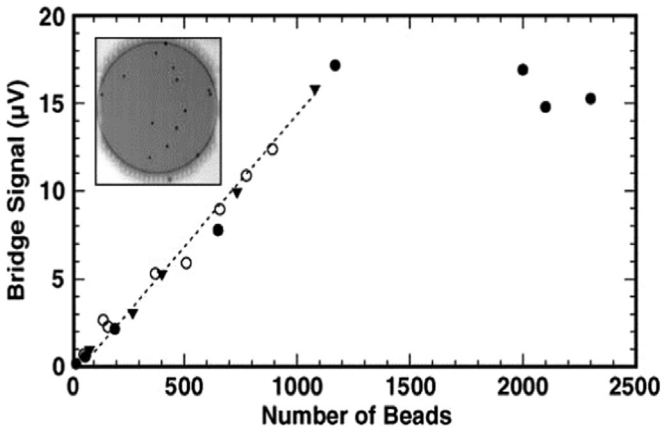

Fig. 14. The output signals of the giant magnetoresistive sensor for detection of different concentration of beads (Rife et al., 2003).

perpendicular GMI effect may be better suited for detecting the magnetic beads. Secondly, to prevent the high-density accumulation of beads, the size of the fixed platform has to be large enough to load all the beads in a single-layer distribution, and the separation distance (between each two beads) needs to be set at least equal to the bead diameter. For example, if a 3×3 mm^2 (3000 μm×3000 μm) Au film is used to immobilize magnetic beads (1 μm), almost 3000×3000 magnetic beads can be immobilized on the Au film. To avoid the offset effect of stray magnetic fields in high-density beads, at least, a bead-diameter distance needs to be set. Roughly speaking, at most 1500×3000 beads are allowed to be immobilized on the Au film.

2.5. The effect of the stray magnetic field of magnetic particles on GMI

Up to now, the physical mechanisms of the enhanced GMI effect, reduced GMI effect or offset GMI effect caused by the magnetic particles are still unclear. Kurlyandskaya et al. (2005) suggest that the enhanced GMI effect can be interpreted as a result of disturbances of the uniform applied magnetic field by the fringe fields of magnetic particles, the presence of stray magnetic fields of the particles changes the superposition of the constant applied field and the alternating field, and thus altering the GMI. Phan et al. (Devkota et al., 2013a) suggest that the major magnetic beads were magnetized in the transverse direction, thus resulting in increased transverse permeability and the enhanced GMI effect. With regard to the enhanced GMI effect, we suggest that the enhanced GMI effect may be caused by the pinning effect of superparamagnetic Dynabeads on the magnetic domain of the sensing elements. The Dynabeads' pinning field may play a role in suppressing the domain-wall movement but strengthening the magnetic moment rotation. Hence, the transverse permeability of soft magnetic layers is greatly increased due to the rotational magnetic permeability modified by the stray magnetic field. In other words, magnetic moment rotation is the main contribution to the enhanced GMI effect at high frequency (Wang et al., 2014a). With regard to the reduced GMI effect, we suggest that the longitudinal stray magnetic field could cause the phenomena of the field inhomogenicity, thereby reducing the effective permeability and thus the GMI effect (Wang et al., 2013a). Until now, the theoretical explanations for the offset GMI effect (Kurlyandskaya et al., 2003; Kurlyandskaya, 2009) are still absent. Qualitatively, we suggest that the presence of the stray magnetic field has strengthened or undermined the external magnetic field, thus shifting the GMI curve.

2.6. Detection of magnetically labeled bioanalytes

Kurlyandskaya (2009) proposed the GMI-based biological analyti-

cal method using the magnetic particles as labels (Kurlyandskaya, 2009). The principles of detecting the magnetically labeled bioanalytes are as follows: the target bioanalytes were first labeled by magnetic particles through functionalization and specific biochemical reactions After applying a magnetic field to magnetize the magnetic particles conjugated with bioanalytes, they can produce a stray magnetic field to modify the GMI of the sensor. Thus, the target bioanalytes can be detected by monitoring the GMI changes induced by the stray magnetic field of magnetic particles.

2.6.1. Detection of human embryonic kidney cells

In 2007, Kurlyandskaya et al. (Kumar et al., 2007) used the CoFeCrSiB ribbon-based GMI sensor to detect the human embryonic kidney (HEK) 293 cells labeled by the magnetic Fe_3O_4 nanoparticles. In this work, Fe_3O_4 nanoparticles were embedded inside human embryonic kidney cells by the intracellular uptake with a concentration of ~10^5 particles/cell, detection of the cells was performed on the ribbon in a contact-type way. Interestingly, the presence of cell-conjugated magnetic nanoparticles on the ribbon had reduced the GMI ratio (Kumar et al., 2007), which is in agreement with that reported in the recent literature (Yuvchenko et al., 2014). This study first introduces the GMI biosensor for detection of magnetic nanoparticles conjugated with bioanalytes, it paves the way for GMI-based biosensing applications.

2.6.2. Detection of the prostate adenocarcinoma cells in rat

Blanc-Béguin et al. (2009) reported that the GMI sensors based on Co-rich amorphous microwires were able to detect Fe_2O_3 nanoparticles conjugated with prostate adenocarcinoma cells in rat. A semi-quantitative analysis was accomplished through detecting different concentrations of cell-adsorbed Fe_2O_3 nanoparticles (0.05–2 mg/ml) on GMI sensitive elements (Blanc-Béguin et al., 2009). This semi-quantitative analysis lays a solid foundation for development of GMI biosensor in determining biomolecules, which shows great *potential* applications in the field of *target detection*.

2.6.3. Genotyping of human papilloma virus type 16/18

Unfortunately, the existent GMI-based biosensing researches mostly focus on detecting magnetic particles, not on the bioanalysis of bioanalytes. To explore the biomedical significance of the GMI effect, quick and parallel genotyping of human papilloma virus (HPV) type 16/18 using the GMI sensor was performed by Zhou et al. (Yang et al., 2010). This study firstly presented a microchannel encapsulated with polydimethylsiloxane (PDMS) for genotyping of human papilloma viruses that were labeled by magnetic nanoclusters through biotin-streptavidin bond, as shown in Fig. 15 (Yang et al., 2010). Importantly, this research focuses on the detection of the bio*targets* rather than the magnetic particles.

2.6.4. Specificity detection of gastric cancer cells

A GMI-based biosensing system combining with the magnetic labeled technology was used to detect gastric cancer cells (Chen et al., 2011). Detailed bioassaies including the preparation and characterization of magnetic Fe_3O_4 nanoparticles, the magnetic labeling procedure and the specific detection of the gastric cancer cells were introduced in this study, as shown in Fig. 16 (Chen et al., 2011). The insight of this research lies in that: Firstly, it provides a typical in-situ testing method based on GMI effect for detecting gastric cancer cells. Secondly, prior to this research, the specificity detection of bioanalytes using GMI sensors had never been systematically studied.

2.6.5. Detection of Curcumin

A MX biosensor based on a HNO_3-treated amorphous ribbon has been used to detect superparamagnetic Fe_3O_4 nanoparticles tagged with Curcumin (Devkota et al., 2014a). Quantification of Curcumin-conjugated Fe_3O_4 nanoparticles was realized at low particle concentrations (0–50 ng/ml). A stable GMI response was observed (Devkota et al., 2014a) when the particle concentration was over 50 ng/ml. This MX biosensor is well suited for supersensitive detection of magnetically labeled bioanalytes. Phan et al. also reported a GMI biosensor based on an amorphous ribbon for detection of Fe_3O_4 nanoparticles functionalized with Curcumin (Devkota et al., 2014b). This study provides essential information for development of GMI biosensor in detecting anticancer drugs.

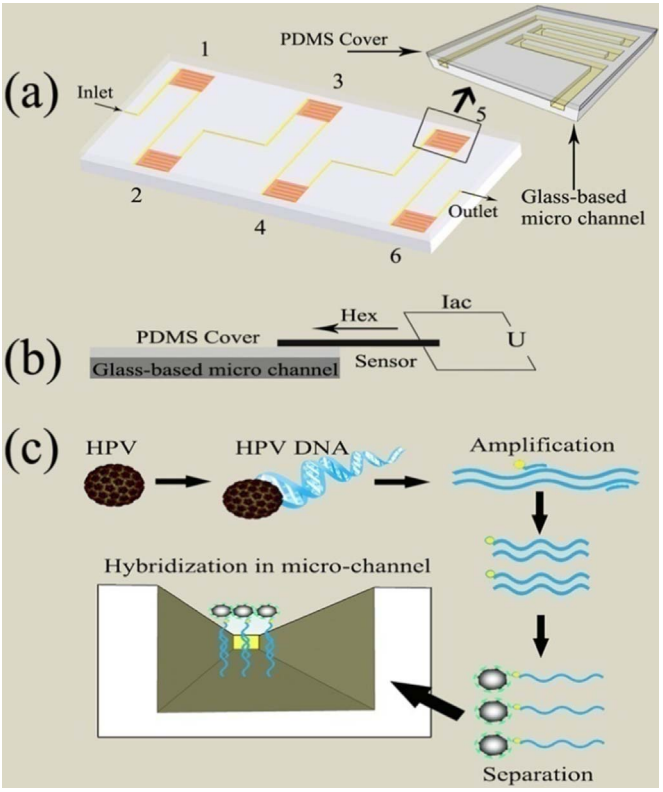

Fig. 15. (a) Schematic diagram of microchannel, (b) Detection principle of GMI-based microchannel system, and (c) Schematic diagram of the microchannel analysis for genotyping of human papilloma virus type 16/18 (Yang et al., 2010).

2.6.6. A MX sensor for detection of Lewis lung carcinoma cancer cells

Lately, Phan et al. presented a MX biosensor based on an acid-treated amorphous ribbon for detecting the manganese oxide (MnO) nanoparticles embedded into Lewis lung carcinoma (LLC) cancer cells (Devkota et al., 2015). It was shown that the sensitivity of the MX sensor can reach almost 3.6% for detecting the MnO nanoparticles at low frequency, which was one order of magnitude higher than that (~0.4%) of MI sensor (Devkota et al., 2015). The MX-based biosensor may be developed as a magnetic resonance imaging tool for diagnosis of cancers.

2.6.7. One-step quick detection of cancer cell surface markers

Bao et al. (2013) reported a GMI sensor based on NiFe/Cu/NiFe films for quick detection of the surface markers of cancer cells labeled by magnetic nanoparticles, involving human lung carcinoma cells (A549), human lung epithelial adenocarcinoma cells (Calu-3), human epithelial cells (HEK293), human epithelial cervix adenocarcinoma cells (Hela), Human umbilical vein endothelial cells (HUVEC) and carcinoma associated lung fibroblasts (CaFbr). Since the films-based GMI sensors are easily applied to mass production and integrating, the obtained results show the potential of GMI sensor in clinical application. Unfortunately, this study only focuses on the qualitative analysis of cell surface markers, quantitative and specific detections of biomarkers are still absent.

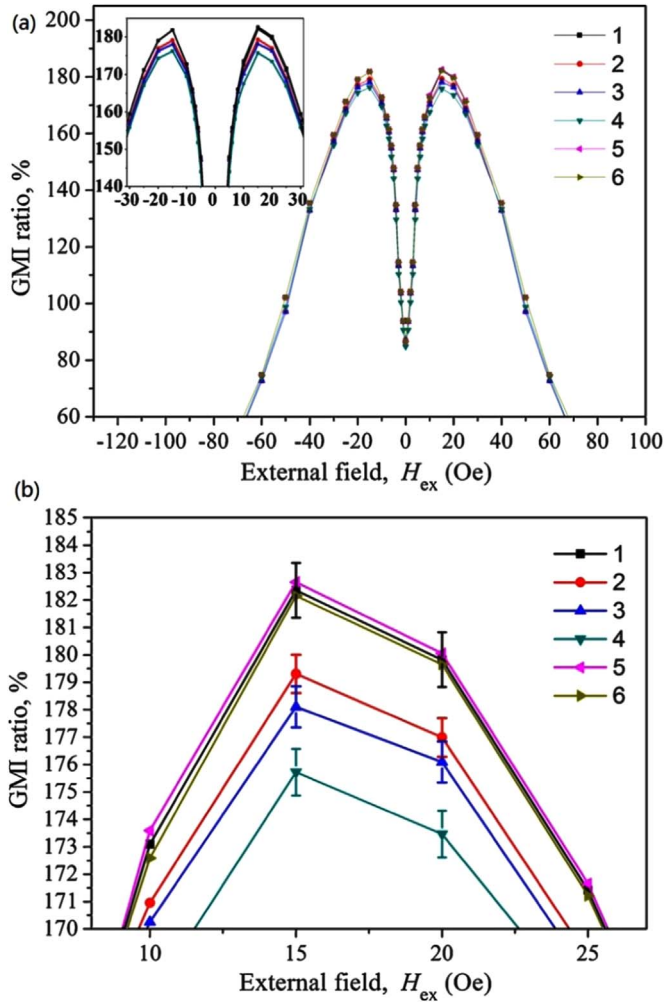

Fig. 16. (a) GMI response of six different samples at a frequency of 10 MHz; (b) Standard deviation analysis of 10 repeated test results of six different samples (1, MGC-803s without nanoparticles; 2, MGC-803s with Fe_3O_4@chitosan; 3, MGC-803s incubated with RGD-Fe_3O_4 @chitosan plus RGD; 4, MGC-803s incubated with RGD-Fe_3O_4@chitosan; 5, GES-1s without nanoparticles; 6, MGC-803s with RGD-4C) (Chen et al., 2011).

2.6.8. In-situ detection of alpha-fetoproteins

Generally speaking, quantitative data, detection limit, linear range and specificity test are needed in a bioassay, but most of which are absent in the early GMI-based bioassaies. In order to explore the biomedical significance of the GMI sensor, we used an integrated GMI sensor based on multilayered films (Cr/Cu/NiFe/Cu/NiFe/Al_2O_3/Cr/Au) involving Dynabeads-labeled sandwich immunoassay for in-situ detection of alpha-fetoprotein (AFP) antigens (Wang et al., 2014c). In this case, all the immunoassay steps were performed on the Au film of the sensor, and there was no contact between the biochemical liquids and the sensitive elements because the Al_2O_3 layer was covered on the soft magnetic films, as shown in Fig. 17(a) (Wang et al., 2014c). Qualitative detection of low-concentration AFP (1 ng/ml and 10 ng/ml) and specific test were realized by using the integrated GMI sensor. Unfortunately, we found it impossible to perform the quantitative detection of AFP antigens by using different electroplating-prepared GMI sensors due to the performance difference between them. Similar results were also reported in another work (Wang et al., 2015a). In order to quantify the biomarker using different GMI sensors, it is required to have the same GMI properties in the GMI sensors. However, it is impossible for us to fabricate identical GMI sensors using the electroplating technology. Nonuniform solution temperature, external magnetic field and current density are influential factors to the uniformity of films. Thus, the electroplated films always have different GMI properties even if they are fabricated in the same batch. Probably the difference in magnetic properties of the electroplated NiFe film is the main cause of different GMI properties. Theoretically, *there* are *two options to perform* quantitative analysis of the biomarkers*: Firstly,* we could choose the sputtered magnetic film or amorphous ribbon as the GMI sensitive elements because they have nearly same magnetic properties. Secondly, since quantification of Dynabeads was achieved by using the separated-type testing method based on one GMI sensor (Wang et al., 2013a), it is possible for us to fulfil the quantitative analysis of the biomarkers using the separated-type testing method. In addition, the separated-type testing method can prevent the chemical solutions from contaminating the sensor. Hence, the GMI sensor can be reused easily without washing. We also used the separated-type testing method to quantify the AFP antigens. The quantitative detection results are shown in Fig. 17(b) and (c), clearly, the GMI ratio increases with increasing AFP concentration from 1 pg/ml to 1 ng/ml. As can be seen from Fig. 17(d), the GMI response is linear with the AFP concentration in the range of 1 pg/ml to 1 ng/ml. Thus, the low-concentration AFP (1 pg/ml to 1 ng/ml) can be determined by using the GMI-based separated-type testing method. The GMI response is not proportional to the AFP concentration while it is over 0.2%. Consequently, the high-concentration AFP antigens cannot be quantified due to the accumulation of high-density Dynabeads. In addition, 1% bovine serum albumin (BSA) was used as a nonspecific target for specificity detection. It was shown that there was no obvious positive signal detected in the experiments due to the presence of 1% BSA. Therefore, the GMI-based magnetic immunoassay is of good specificity.

2.6.9. Supersensitive detection of alpha-fetoprotein and carcinoembryonic antigens

In the following work (Wang et al., 2015b), a GMI-based separated-type testing method was used to quantify carcinoembryonic antigens (CEA) that were captured in a Micro-cavity consisting of Au film and SU-8 photoresist. Quantification of low-concentration CEA (1 pg/ml to 10 ng/ml) was achieved by using the GMI sensor, and the minimum detectable concentration for CEA can be as low as 1 pg/ml, as shown in Fig. 18 (Wang et al., 2015b). On the one hand, Since the high-concentration biomolecules can conjugate a large number of magnetic particles, which also induces the cancellation effect in particles' stray magnetic fields, it is infeasible to quantify the high-concentration CEA (> 10 ng/ml) due to the high-density cluster of Dynabeads (Lodewijk et al., 2014; Chiriac et al., 2005; Devkota et al., 2013b; Wang et al., 2014b). On the other hand, washing steps are needed after labeling the biomolecules by magnetic particles. Therefore, the accumulation of magnetic particles is absent, which weakens the cancellation effect when high-concentration biomolecules are tested. As you can see Fig. 18(c), the GMI response shows a good linear relationship with CEA concentration in the range of 1 pg/ml to 10 ng/ml. Consequently, the GMI sensor is particularly suited for ultrasensitive detection of low-concentration biomarkers.

As can be seen from Fig. 17 and Fig. 18, the upper detection limit for AFP antigens (1 ng/ml) is much lower than that for CEA antigens (10 ng/ml). This is because the actual number of AFP antigens is much more than the number of CEA antigens under the same volumes of solution. Consequently, AFP sample can bind with more beads than CEA sample under equal-volume solution.

2.6.10. Detection of Escherichia coli O157:H7

Recently, we used a GMI biosensor to detect the Escherichia coli O157:H7 (Yang et al., 2015c, 2016). In the experiment, Escherichia coli was captured and labeled with Dynabeads by sandwich assay combined with biotin-streptavidin bond on several Au films. Different-concentration Escherichia coli (100, 300 and 500 cfu/ml) was first immobilized on Au films, and then placed on the surface of GMI sensor for no-contact testing, respectively. *It* has been *shown that* the GMI

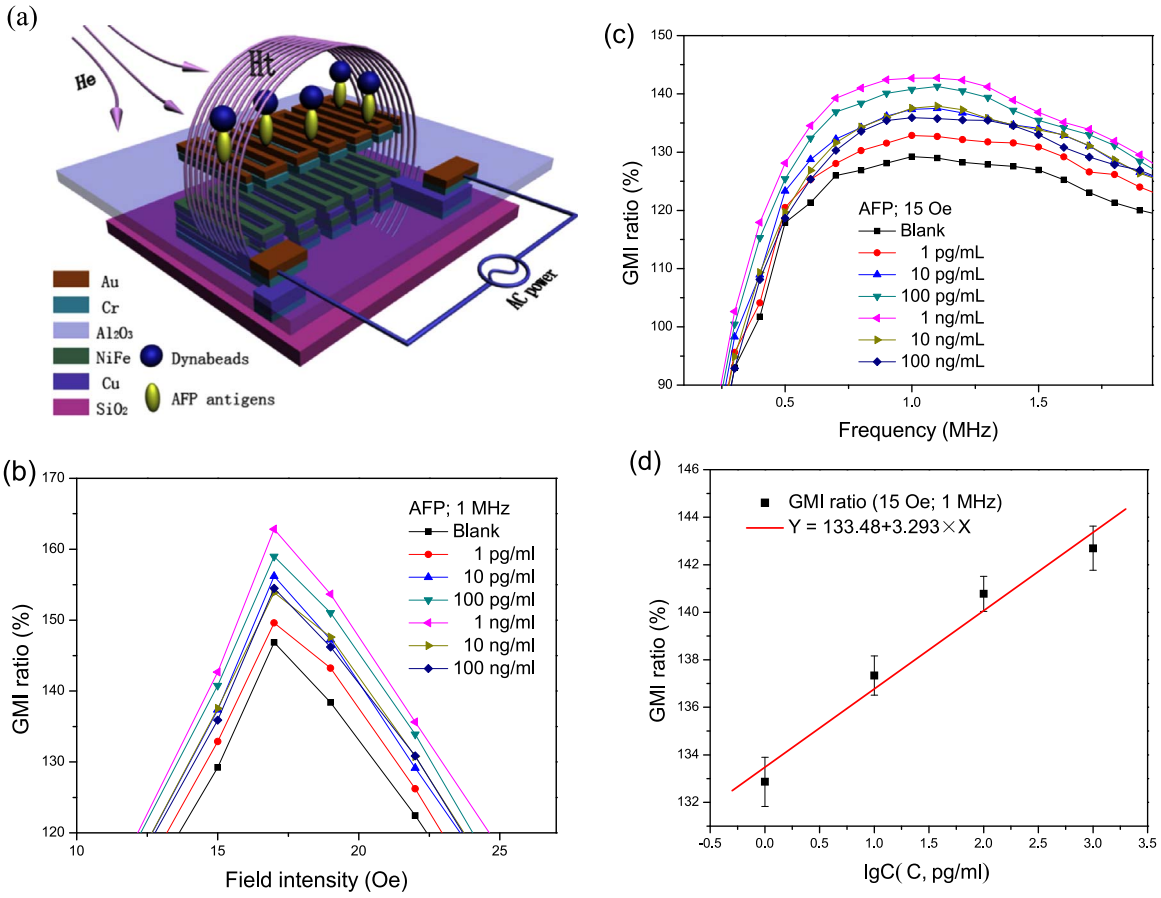

Fig. 17. (a) Schematic diagram of AFP detection using the in-situ testing method; (b) Magnetic field dependency of GMI response for quantification of AFP antigens (1 pg/ml to 100 ng/ml) using the separated-type testing method; (b) Frequency dependency of GMI response for quantification of AFP antigens (1 pg/ml to 100 ng/ml) using the separated-type testing method (d) The linear relationship between AFP concentration and GMI response (Wang et al., 2014c).

ratio was significantly improved due to the presence of Dynabeads-labeled Escherichia coli, and the GMI ratio increased with increasing the concentration of Escherichia coli. Later, the Escherichia coli was labeled with Dynabeads on the Au film in a open-surface microfluidic cavity which was composed of SU-8 photoresist, then, the open-surface microfluidic cavity was immobilized on the edge of GMI sensor for testing (Yang et al., 2016), as shown in Fig. 19 (a), (b) and (c). Quantification of the Escherichia coli was realized by using a separated-type testing method based on GMI effect, as shown in Fig. 19 (d) (Yang et al., 2016). This study opens a new way for quantification of Escherichia coli, which is very useful for development of GMI-based microfluidic cavity in determining bacterium.

2.6.11. Quantitative determination of C-reactive protein

In 2015, C-reactive protein (CRP) was detected by using an Au-coated GMI biosensor (Yang et al., 2015b), as shown in Fig. 20 (a) and (b). Sandwich assay combined with biotin-streptavidin assay was carried out on the Au film of the GMI biosensor for labeling the CRP with Dynabeads. Quantitative determination of CRP was achieved in the CRP concentration range of 1–10 ng/ml, as shown in Fig. 20 (c) (Yang et al., 2015b), demonstrating a good linear relationship between the GMI response and the CRP concentration.

Until now, AFP, CEA, CRP, HPV type 16/18, HEK 293 cells, gastric cancer cells, A549, Calu-3, HEK293, Hela, HUVEC, CaFbr and Escherichia coli O157:H7 have been detected by using the GMI biosensor combined with magnetic labeling technique. The results of detecting magnetically labeled bioanalytes were summarized in Table 1.

2.7. Label-free detection

2.7.1. The modification effect on GMI

One of the label-free biologic detection is based on monitoring the GMI changes that are caused by the modification effect of biochemical reagents on the sensitive element. In other words, the geometry, surface morphology or surface anisotropy of the sensitive element can be modified when it is exposed to the biochemical reagents, thus altering the GMI response of the sensor.

Kurlyandskaya and Miyar (2007) have studied the GMI effect of the FeCoSiB ribbon whose surface was modified with human urine. Great changes have taken place in GMI due to the modification effect on the ribbon, as shown in Fig. 21. In order to develop label-free magnetoimpedance spectroscopy which can be used for monitoring the surface effect of magnetic electrodes, the influence of surface modification of as-quenched FeCoSiB ribbons and FeCoCrSiB ribbons on GMI effects was studied by measuring the GMI responses of them in different corrosive fluids (Kurlyandskaya et al., 2007): distilled water, physiological solution, phosphate buffer saline, and orthophosphoric acid. It can be observed that there was a noticeable transformation in the GMI effect after modifying the ribbons with orthophosphoric acid (Kurlyandskaya et al., 2007). The observed effects can be explained as that the orthophosphoric acid has changed both the thickness and the effective magnetic anisotropy of the ribbons, and thus the GMI effect. Therefore, it is possible to develop a GMI biosensor based on the principle of electrochemical magnetoimpedance spectroscopy for direct detection of the biochemical liquids.

To explore label-free magnetic sensing technology based on GMI effect, the acid-modification effect on GMI in a CoFeNiSiB amorphous ribbon has been investigated systematically (Devkota et al., 2014c). It

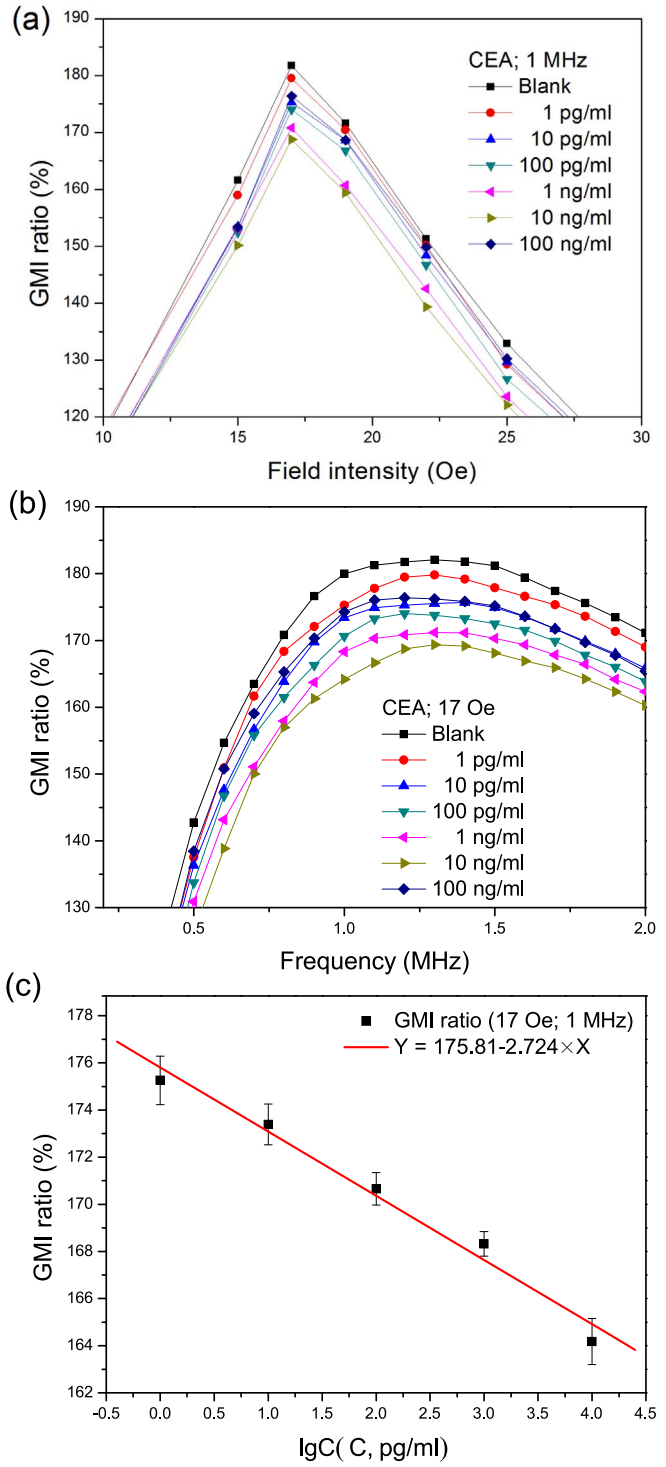

Fig. 18. Detection of CEA antigens (1 pg/ml to 100 ng/ml) using the separated-type testing method (a) Magnetic field dependency of GMI ratio; (b) Frequency dependency of GMI ratio; (c) The linear relationship between CEA concentration and GMI response (Wang et al., 2015b).

was shown that the GMI response decreased in all the acid-treated ribbon relative to their plain sample (Devkota et al., 2014c), and the GMI response decreased with increasing concentration of the treated acid. This can be understood by considering the fact that the surface irregularity of the ribbon is increased since it is etched with a stronger acid, the transverse permeability is thus greatly reduced, and leading to the reduced GMI effect. The results are of practical importance in developing label-free GMI detector for monitoring the state of acid-based solutions.

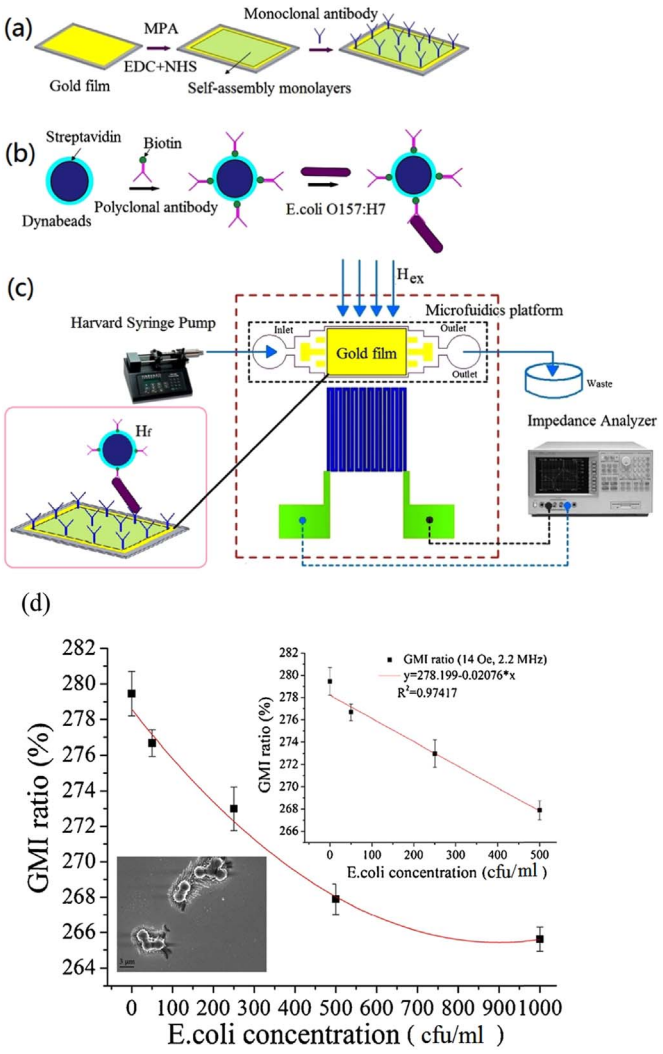

Fig. 19. (a) Surface modification of gold film; (b) Immunoassay for capturing and labeling Escherichia coli; (c) Graphical illustration of the experimental setup; (d) GMI responses in relation to the Escherichia coli concentration (Yang et al., 2015c, 2016).

2.7.2. *Detection of the biomagnetic fields in living systems*

In 2009, detection of the biomagnetic field for both the human body and the selected tissue sample were carried out by using a GMI sensor based on an amorphous wire (Uchiyama et al., 2009). Unlike the particles-labeled biosensing technology, the GMI sensor was directly used to detect the biomagnetic fields in biological tissues. The GMI sensor can not only detect the magnetic cardiogram signals but also the localized biomagnetic fields generated by the biologic samples with millimetre size, reaching a detection sensitivity of pico-Tesla (Uchiyama et al., 2009). Later, Nakayama et al. and Uchiyama et al. reported a GMI biosensor based on a CoFeSiB amorphous wire for detecting the biomagnetic fields in the musculatures of the stomach in a guinea-pig with spontaneous electric activity (Nakayama et al., 2011; Uchiyama et al., 2011). Since the musculatures only produce very weak magnetic fields (pico-Tesla level) due to their organic compounds, a highly sensitive biosensing system consisting of sample-and-hold circuits, power supply, high/low-pass filters, GMI sensitive element, analog-digital converter was established to detect the biomagnetic fields of the musculatures (Nakayama et al., 2011; Uchiyama et al., 2011). This GMI sensor with the sensitivity of a pico-Tesla level enabled quasi-real time recordings of the magnetic fields for biological

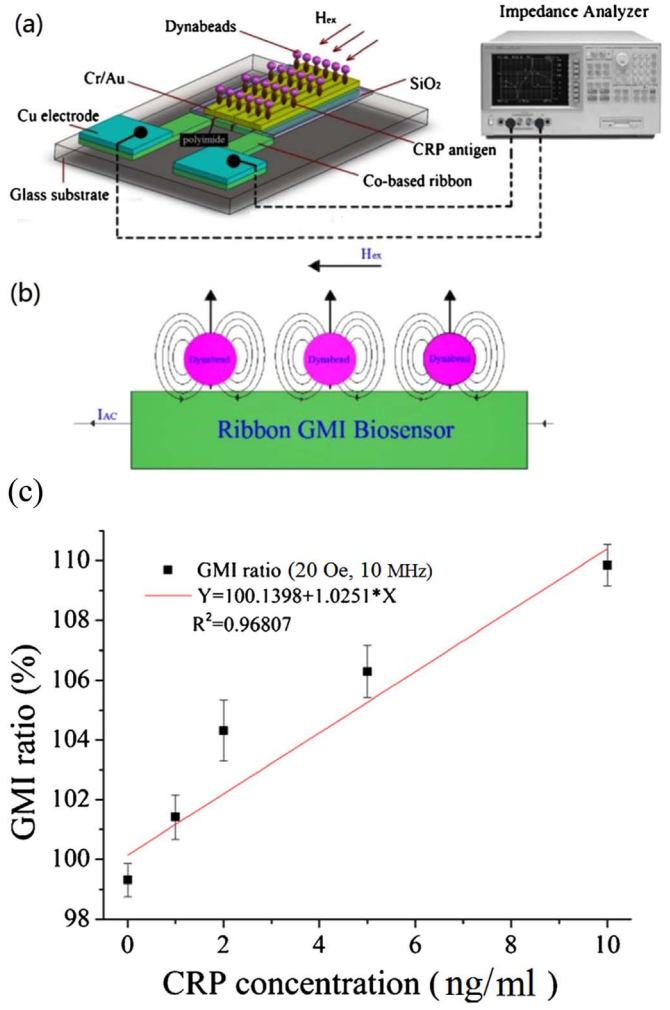

Fig. 20. (a) Schematic of testing CRP using the Au-coated GMI biosensor; (b) Magnetization of Dynabeads (c) GMI responses in relation to the CRP concentration (Yang et al., 2015b).

electric activity because of the sufficient short operation interval (1 μs). The detection results are shown in Fig. 22. The findings indicate that the GMI sensor *is* a *promising* tool *for non-invasive* detection of cell activity or function through the biomagnetic measurements, which could be an effective non-invasive method for diagnosis of diseases with high sensitivity.

3. Concluding remarks and future perspectives

The use of high-concentration biomolecules can induce the high-density aggregation or even cluster of the particles. The adjacent exciting fields of the particles will cancel each other out due to the agglomeration of particles, which make the GMI sensor infeasible to perform quantitative analysis. In order to detect high-concentration magnetic particles, three main issues need to be sorted out: Firstly, the particles are not dispersed after dropping them on a testing platform. It is necessary to disperse the particles after dropping them on a testing platform. Secondly, the testing platform is too small to load the particles. To prevent the high-density accumulation of the particles, the size of the testing platform needs to be large enough to load all the particles in a single-layer distribution, and the separation distance (between each two beads) is set at least equal to the particle diameter. Thirdly, the magnetic particles cannot be distributed uniformly on a flat surface is also an important factor. Since the perpendicular magnetic field can make the magnetic particles distribute uniformly

Table 1
The results of detecting the magnetically labeled bioanalytes based on GMI biosensors.

Target bioanalytes	Specificity and qualitative analysis	Linearity range	Upper detection limit	Lower detection limit	References
AFP	Good specificity (1% BSA)	1 pg/ml to 1 ng/ml	1 ng/ml	1 pg/ml	Wang et al., 2014c
CEA		1 pg/ml to 10 ng/ml	10 ng/ml	1 pg/ml	Wang et al., 2015b
CRP		1 ng/ml to 10 ng/ml	10 ng/ml	1 ng/ml	Yang et al., 2015b
Coli O157: H7		50 cfu/ml to 500 cfu/ml	500 cfu/ml	50 cfu/ml	Yang et al., 2016
Gastric cancer cells MGC-803	Good specificity (80% confluent)				Chen et al., 2011
HPV 16/18	Good specificity	4 copies to 400 copies	400 copies	4 copies	Yang et al., 2010
A549, Calu-3, HEK293, Hela, HUVEC, CaFbr	Qualitative results (12.0%, 3.7%, 14.0%, 6.6%, 84.5%, 12.5%)				Bao et al., 2013

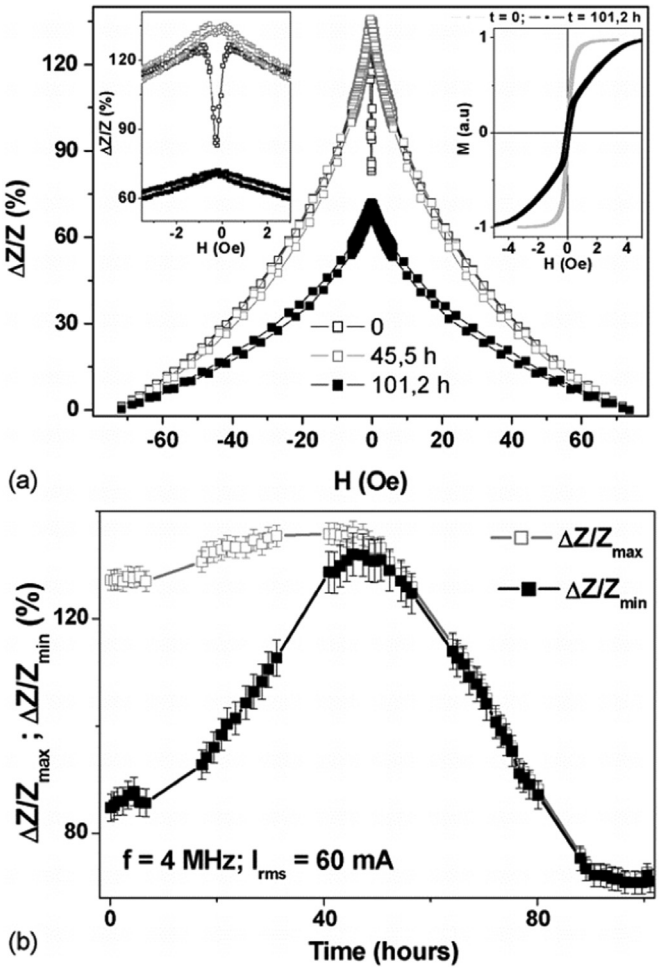

Fig. 21. GMI responses of the FeCoSiB ribbons modified with human urine (a) Field dependency under different modification time; (b) Time-dependent modification results (Kurlyandskaya and Miyar, 2007).

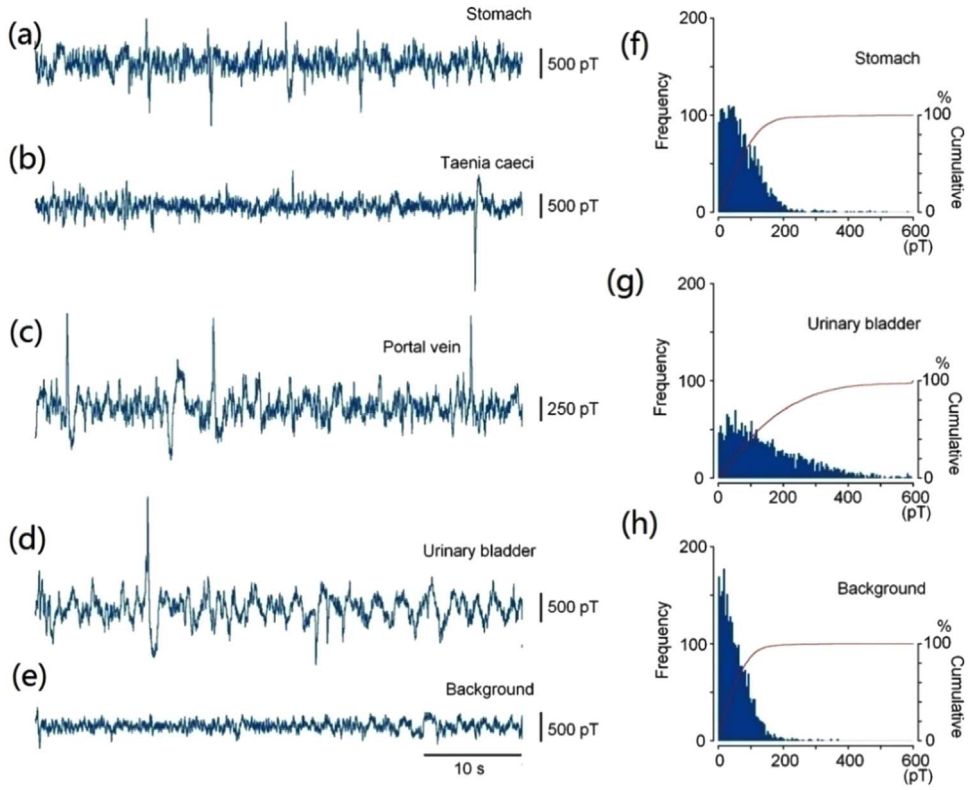

Fig. 22. Magnetic activities recorded from various smooth muscle musculature preparations. (a)–(d) Examples of magnetic activities for 50 s in the stomach, taenia caeci, portal vein and urinary bladder, respectively. (e) Background noise. (f)–(h) Amplitude histograms constituted from the magnetic recordings of (a), (d) and (e), respectively. Red curves represent cumulative (%) of the histograms. Bin width=5 pT (Nakayama et al., 2011; Uchiyama et al., 2011). (For interpretation of the references to color in this figure legend, the reader is referred to the web version of this article.)

on a flat surface, the perpendicular GMI effect in films or ribbons may be more suitable for on-chip (in-situ) biosensing applications. Moreover, the perpendicular magnetization method is probably also suited for use in the magnetoresistance-based biosensing applications such as Giant magnetoresistance, Tunnel magnetoresistance, Anisotropic magnetoresistance. However, the microwire-based GMI sensor is not appropriate for on-chip (in-situ) magnetic labeling detection due to its circular structure.

Enhanced GMI effect, reduced GMI effect and offset GMI effect were observed in the presence of magnetic particles on the GMI sensor (with and without the protective layer) or near the GMI sensor. Nevertheless, the physical mechanisms of these phenomena are still not clear. In order to thoroughly understand the effect of the stray magnetic field of particles on GMI, an accurate theoretical model needs to be established in future work. More confirmatory experiments such as the magnetic domain observations after coating the magnetic particles on the sensitive elements (with and without the protective layer) or immobilizing the magnetic particles near the sensitive elements are needed in the further research.

There are several ways to improve the sensitivity of the GMI sensor for detection of magnetically labeled bioanalytes. Wire: As the coupled microwires can obtain enhanced detection sensitivity, the microwire array is a better choice in magnetic bioanalysis. Film: it is better to use the multilayer structure to detect magnetic particles due to its high field-sensitivity. Ribbon: the detection sensitivity can be improved significantly by using the acid-treated ribbons.

In order improve the detection efficiency and sensitivity, it is better to quantify the biomolecules using different GMI sensor and on-chip testing method. The soft magnetic films are more suitable for fabrication of GMI biosensors because they own more optimal structure, better homogeneity and integrating than the wires and ribbons. Until now, it is difficult to fabricate the homogeneous GMI sensors based on films using the electroplating technology owing to its instability. Alternatively, the sputtered magnetic film is probably a better choice for GMI-based biosensing applications because they have nearly the same magnetic properties.

Detections of AFP antigens, CEA antigens, CRP antigens, HPV type 16/18, HEK 293 cells, gastric cancer cells, A549, Calu-3, HEK293, Hela, HUVEC, CaFbr and Escherichia coli O157:H7 were achieved by using the GMI sensor combined with the magnetic labeling technique. These results lay solid foundations for clinical applications of the GMI sensor. The minimum detectable concentration for CEA antigens and AFP antigens can both be as low as 1 pg/ml, thus, the GMI sensor is very promising for supersensitive detection of the low-concentration biomarkers. The next step is to detect these biological targets in the human blood or tissues, and to explore the possibility of using the GMI sensor in clinical diagnosis.

The GMI-based biosensing system is capable of detecting the biomagnetic fields in the musculatures of the stomach, taenia caeci, portal vein and urinary bladder of a guinea-pig. The biomagnetic field of human musculatures is roughly equivalent to that of the guinea-pig, alternately, the next step is to detect the biomagnetic field in the musculatures of human organs using the GMI sensor. Furthermore, the GMI sensor may be used to screen the lesions of human musculatures through detecting the difference in the biomagnetic fields of musculatures tissues of different organs.

Acknowledgments

This work is supported by The National Natural Science Foundation of China (No. 61273065), National Natural Science Foundation of China (No. 61525305), National Natural Science Foundation of China (No. 51575333), Science and Technology Commission of Shanghai (No. 16441909400), Natural Science Foundation of Shanghai (13ZR1420800), Support fund of Shanghai Jiao Tong University (AgriX2015005), Support fund of Joint research center for advanced

aerospace technology of Shanghai Academy of Spaceflight Technology-Shanghai Jiao Tong University (USCAST2015-2), Support fund of Aerospace Technology (15GFZ-JJ02-05), the Analytical and Testing Center in Shanghai Jiao Tong University, the Center for Advanced Electronic Materials and Devices in Shanghai Jiao Tong University.

References

Albisetti, E., Petti, D., Cantoni, M., Damin, F., Torti, A., Chiari, M., Bertacco, R., 2013. Biosens. Bioelectron. 47, 213–217.

Albon, C., Weddemann, A., Auge, A., Rott, K., Hütten, A., 2009. Appl. Phys. Lett. 95 (2), 023101.

Amirabadizadeh, A., Lotfollahi, Z., Zelati, A., 2016. J. Magn. Magn. Mater. 415, 102–105.

Bao, C.C., Chen, L., Wang, T., Lei, C., Tian, F.R., Cui, D.X., Zhou, Y., 2013. Nano-Micro Lett. 5, 213–222.

Baselt, D.R., Lee, G.U., Natesan, M., Metzger, S.W., Sheehan, P.E., Colton, R.J., 1998. Biosens. Bioelectron. 13, 731–739.

Beach, R.S., Berkowitz, A.E., 1994. Appl. Phys. Lett. 64 (26), 3652–3654.

Berensmeier, S., 2006. Appl. Microbiol. Biotechnol. 73 (3), 495–504.

Besse, P.A., Boero, G., Demierre, M., Pott, V., Popovic, R., 2002. Appl. Phys. Lett. 80 (22), 4199–4201.

Bi, S., Zhang, Z.P., Dong, Z., Wang, Z.H., 2015. Biosens. Bioelectron. 65, 139–144.

Blanc-Béguin, F., Nabily, S., Gieraltowski, J., Turzo, A., Querellou, S., Salaun, P., 2009. J. Magn. Magn. Mater. 321, 192–197.

Chen, L., Bao, C.C., Yang, H., Li, D., Lei, C., Wang, T., Hu, H.Y., He, M., Zhou, Y., Cui, D.X., 2011. Biosen. Bioelectron. 26, 3246–3253.

Chiriac, H., Tibu, M., Moga, A., Herea, D., 2005. J. Magn. Magn. Mater. 293, 671–676.

Chiriac, H., Herea, D., Corodeanu, S., 2007. J. Magn. Magn. Mater. 311, 425–428.

Choi, J., Gani, A.W., Bechstein, D.J., Lee, J.R., Utz, P.J., Wang, S.X., 2016. Biosens. Bioelectron. 85, 1–7.

De Boer, B.M., Kahlman, J.A.H.M., Jansen, T.P.G.H., Duric, H., Veen, J., 2007. Biosens. Bioelectron. 22 (9), 2366–2370.

Denoual, M., Harnois, M., Saez, S., Dolabdjian, C., Senez, V., 2011. International Solid-State Sensors, Actuators and Microsystems Conference. 16, pp. 80–83.

Devkota, J., Ruiz, A., Mukherjee, P., Srikanth, H., Phan, M.H., 2013a. IEEE Trans. Magn. 49, 4060–4063.

Devkota, J., Wang, C., Ruiz, A., Mohapatra, S., Mukherjee, P., Srikanth, H., Phan, M.H., 2013b. J. Appl. Phys. 113, 104701.

Devkota, J., Wingo, J., Mai, T.T.T., Nguyen, X.P., Huong, N.T., Mukherjee, P., Srikanth, H., Phan, M.H., 2014a. J. Appl. Phys. 115, 17B503.

Devkota, J., Trang, M.T., Stojak, K., Ha, P.T., Pham, H.N., Nguyen, X.P., Mukherjee, P., Srikanth, H., Phan, M.H., 2014b. Sens. Actuators B Chem. 190, 715–722.

Devkota, J., Huong, N.T., Srikanth, H., Phan, M.H., 2014c. IEEE Trans. Magn. 50 (6), 1–4.

Devkota, J., Howell, M., Mukherjee, P., Srikanth, H., Mohapatra, S., Phan, M.H., 2015. J. Appl. Phys. 117, (17D123).

Drozdov, A.S., Ivanovski, V., Avnir, D., Vinogradov, V.V., 2016. J. Colloid Interface Sci. 468, 307–312.

Drung, D., ABmann, C., Beyer, J., Kirste, A., Peters, M., Ruede, F., Schurig, T., 2007. IEEE Trans. Appl. Supercond. 17 (2), 699–704.

Ejsing, L., Hansen, M.F., Menon, A.K., Ferreira, H.A., Graham, D.L., Freitas, P.P., 2004. Appl. Phys. Lett. 84, 4729–4731.

Ferreira, H.A., Graham, D.L., Freitas, P.P., Cabral, J.M.S., 2002. J. Appl. Phys. 93, 7281–7286.

Fodil, K., Denoual, M., Dolabdjian, C., Harnois, M., Senez, V., 2013. IEEE Trans. Magn. 49 (1), 93–96.

Fodil, K., Denoual, M., Dolabdjian, C., Treizebre, A., Senez, V., 2014. IEEE Trans. Magn. 50 (4), 1–8.

Fodil, K., Denoual, M., Dolabdjian, C., 2016a. IEEE Trans. Magn. 52 (1), 1–9.

Fodil, K., Denoual, M., Dolabdjian, C., Treizebre, A., Senez, V., 2016b. Appl. Phys. Lett. 108 (17), 173701.

Fuentes, M., Mateo, C., Guisan, J.M., Fern ´ andez-Lafuente, R., 2005. Biosens. Bioelectron. 20, 1380–1387.

García-Arribas, A., Martínez, F., Fernández, E., Ozaeta, I., Kurlyandskaya, G.V., Svalov, A.V., Barandiaran, J.M., 2011. Sens. Actuators A 172 (1), 103–108.

Gaster, R.S., Hall, D.A., Nielsen, C.H., Osterfeld, S.J., Yu, H., Mach, K.E., Wilson, R.J., Murmann, B., Liao, J.C., Gambhir, S.S., Wang, S.X., 2009. Nat. Med. 15 (11), 1327–1332.

Graham, D.L., Ferreira, H., Bernardo, J., Freitas, P.P., Cabral, J.M.S., 2002. J. Appl. Phys. 91 (10), 7786–7788.

Graham, D.L., Ferreira, H.A., Freitas, P.P., Cabral, J.M.S., 2003. Biosens. Bioelectron. 18 (4), 483–488.

Hall, D.A., Gaster, R.S., Osterfeld, S.J., Murmann, B., Wang, S.X., 2010. Biosens. Bioelectron. 25 (9), 2177–2181.

Hao, L., Aßmann, C., Gallop, J.C., Cox, D., Ruede, F., Kazakova, O., Josephs-Franks, P., Drung, D., Schurig, T., 2011. Appl. Phys. Lett. 98 (9), 092504.

Heim, E., Ludwig, F., Schilling, M., 2009. J. Magn. Magn. Mater. 321, 1628–1631.

Huang, G., Zhou, B., Chen, Z., Jiang, H., Xing, X., 2015. IEEE Sens. J. 15 (1), 333–336.

Jackson, J.D., 1975. Classical Electrodynamics. John Wiley & Sons, Inc., USA.

Jahanbani, S., Benvidi, A., 2016. Biosens. Bioelectron. 85, 553–562.

Jiang, Z., Llandro, J., Mitrelias, T., Bland, J.A.C., 2006. J. Appl. Phys. 99 (8), 08S105.

Knobel, M., Pirota, K.R., 2002. J. Magn. Magn. Mater. 242, 33–40.

Koets, M., Van der Wijk, T., Van Eemeren, J.T.W.M., Van Amerongen, A., Prins, M.W.J., 2009. Biosens. Bioelectron. 24 (7), 1893–1898.

Kumar, A., Mohapatra, S., Fal-Miyar, V., Cerdeira, A., Garcia, J., Srikanth, H., Gass, J., Kumar, A., Mohapatra, S., Fal-Miyar, V., Cerdeira, A., Garcia, J.A., Srikanth, H., Kurlyandskaya, G.V., 2007. Appl. Phys. Lett. 91 (14), 143902.

Kurlyandskaya, G.V., 2009. J. Magn. Magn. Mater. 321, 659–662.

Kurlyandskaya, G.V., Levit, V., 2005. Biosens. Bioelectron. 20, 1611–1616.

Kurlyandskaya, G.V., Levit, V., 2007a. Mater. Sci. Eng. C 27, 495–503.

Kurlyandskaya, G.V., Miyar, V.F., 2007b. Biosens. Bioelectron. 22, 2341–2345.

Kurlyandskaya, G.V., Sánchez, M.L., Hernando, B., Prida, V.M., Gorria, P., Tejedor, M., 2003. Appl. Phys. Lett. 82, 3053–3055.

Kurlyandskaya, G.V., Miyar, V.F., Saad, A., Asua, E., Rodriguez, J., 2007c. J. Appl. Phys. 101 (5), 054505.

Kurlyandskaya, G.V., Jantaratana, P., Bebenin, N.G., Vas'kovskiy, V.O., 2012. Solid State Phenom. 190, 581–584.

Kurlyandskaya, G.V., Fernández, E., Safronov, A., Svalov, A., Beketov, I., Beitia, A.B., García-Arribas, A., Blyakhman, F., 2015. Appl. Phys. Lett. 106, 193702.

Landau, L.D., Lifshitz, E.M., 1975. Electrodynamics of Continuous Media. Pergamon Press, Oxford.

Lee, C.P., Lai, M.F., Huang, H.T., Lin, C.W., Wei, Z.H., 2014. Biosens. Bioelectron. 57, 48–53.

Lee, W., Joo, S.J., Sun, U.K., Rhie, K.W., Hong, J.K., Shin, K.H., Kim, K.H., 2009a. Appl. Phys. Lett. 94, 153903.

Li, F., Kosel, J., 2014. Biosens. Bioelectron. 59, 145–150.

Liang, R.P., Yao, G.H., Fan, L.X., Qiu, J.D., 2012. Anal. Chim. Acta 737, 22–28.

Lodewijk, K.J., Fernandez, E., Garcia-Arribas, A., Kurlyandskaya, G.V., Lepalovskij, V.N., Safronov, A.P., Kooi, B.J., 2014. J. Appl. Phys. 115 (17), (17A323).

Lu, M., Ibraimi, F., Kriz, D., Kriz, K., 2006. Biosens. Bioelectron. 21 (12), 2248–2254.

Ludwig, F., Heim, E., Mäuselein, S., Eberbeck, D., Schilling, M., 2005a. J. Magn. Magn. Mater. 293 (1), 690–695.

Ludwig, F., Mäuselein, S., Heim, E., Schilling, M., 2005b. Rev. Sci. Instrum. 76 (10), 106102.

Manteca, A., Mujika, M., Arana, S., 2011. Biosens. Bioelectron. 26 (8), 3705–3709.

Manzin, A., Nabaei, V., Kazakova, O., 2012. J. Appl. Phys. 111 (7), (07E513).

Martins, V.C., Cardoso, F.A., Loureiro, J., Mercier, M., Germano, J., Cardoso, S., Freitas, P.P., 2008. AIP Conference Proceedings 1025, pp. 150–175.

Martins, V.C., Cardoso, F.A., Germano, J., Cardoso, S., Sousa, L., Piedade, M., Fonseca, L.P., 2009. Biosens. Bioelectron. 24 (8), 2690–2695.

Matz, H., Drung, D., Hartwig, S., Groß, H., Kötitz, R., Müller, W., Vass, A., Weitschies, W., Trahms, L., 1999. Appl. Supercond. 6 (10), 577–583.

Miller, M.M., Sheehan, P.E., Edelstein, R.L., Tamanaha, C.R., Zhong, L., Bounnak, S., Whitman, L.J., Colton, R.J., 2001. J. Magn. Magn. Mater. 225 (1), 138–144.

Miller, M.M., Prinz, G.A., Cheng, S.F., Bounnak, S., 2002. Appl. Phys. Lett. 81 (12), 2211–2213.

Morikawa, T., Nishibe, Y., Yamadera, H., Nonomura, Y., Takeuchi, M., Sakata, J., 1996. IEEE Trans. Magn. 32, 4965–4967.

Mujika, M., Arana, S., Castano, E., Tijero, M., Vilares, R., Ruano-Lopez, J.M., Berganza, J., 2009. Biosens. Bioelectron. 24 (5), 1253–1258.

Nakayama, S., Atsuta, S., Shinmi, T., Uchiyama, T., 2011. Biosens. Bioelectron. 27 (1), 34–39.

Ng, E., Nadeau, K.C., Wang, S.X., 2016. Biosens. Bioelectron. 80, 359–365.

Oh, S., Jadhav, M., Lim, J., Reddy, V., Kim, C., 2013. Biosens. Bioelectron. 41, 758–763.

Østerberg, F.W., Rizzi, G., de la Torre, T.Z.G., Strömberg, M., Strømme, M., Svedlindh, P., Hansen, M.F., 2013. Biosens. Bioelectron. 40 (1), 147–152.

Palecek, E., Fojta, M., 2007. Talanta 74 (3), 276–290.

Panina, L.V., Mohri, K., 1994. Appl. Phys. Lett. 65, 1189–1191.

Panina, L.V., Mohri, K., Uchiyama, T., Noda, M., 1995. IEEE Trans. Magn. 31, 1249–1260.

Pannetier, L.M., Parkkonen, L., Sergeeva, C.N., Polovy, H., Fermon, C., Fowley, C., 2011. Appl. Phys. Lett. 98, 153705.

Paul, B.K., Bhattacharjee, K., Bose, S., Guchhait, N., 2012. Phys. Chem. Chem. Phys. 14 (44), 15482–15493.

Pflipsen, C., Forge, D., Benali, S., Gossuin, Y., 2013. J. Phys. Chem. C 117 (40), 20919–20926.

Phan, M.H., Peng, H.X., 2008. Prog. Mater. Sci. 53, 323–420.

Phan, M.H., Peng, H.X., Yu, S.C., Vazquez, M., 2006. J. Appl. Phys. 99 (8), (08C505).

Richardson, J., Hill, A., Luxton, R., Hawkins, P., 2001. Biosens. Bioelectron. 16 (9), 1127–1132.

Rife, J.C., Miller, M.M., Sheehan, P.E., Tamanaha, C.R., Tondra, M., Whitman, L.J., 2003. Sens. Actuators A 107 (3), 209–218.

Rizzi, G., Østerberg, F.W., Dufva, M., Hansen, M.F., 2014. Biosens. Bioelectron. 52, 445–451.

Rong, Z., Wang, C., Wang, J., Wang, D., Xiao, R., Wang, S., 2016. Biosens. Bioelectron. 84, 15–21.

Sandhu, A., Kumagai, Y., Lapicki, A., Sakamoto, S., Abe, M., Handa, H., 2007. Biosens. Bioelectron. 22 (9), 2115–2120.

Serrate, D., De Teresa, J.M., Marquina, C., Marzo, J., Saurel, D., Cardoso, F.A., Ibarra, M.R., 2012. Biosens. Bioelectron. 35 (1), 206–212.

Shen, W., Liu, X., Mazumdar, D., Xiao, G., 2005. Appl. Phys. Lett. 86 (25), 253901.

Shoshi, A., Schotter, J., Schroeder, P., Milnera, M., Ertl, P., Heer, R., Brueckl, H., 2013. Biosens. Bioelectron. 40 (1), 82–88.

Sinha, B., Ramulu, T.S., Kim, K.W., Venu, R., Lee, J.J., Kim, C.G., 2014. Biosens. Bioelectron. 59, 140–144.

Srinivasan, B., Li, Y., Jing, Y., Xu, Y., Yao, X., Xing, C., Wang, J.P., 2009. Angew. Chem. Int. Ed. Engl. 48 (15), 2764–2767.

Stevenson, A.C., Araya-Kleinsteuber, B., Sethi, R.S., Metha, H.M., Lowe, C.R., 2005. Biosens. Bioelectron. 20 (7), 1298–1304.

Sun, Y., Bi, N., Song, D.Q., Bai, Y., Wang, L.Y., Zhang, H.Q., 2008. Anal. Chim. Acta 624, 294–300.
Uchiyama, T., Nakayama, S., Mohri, K., Bushida, K., 2009. Phys. Status Solidi A 206, 639–643.
Uchiyama, T., Mohri, K., Nakayama, S., 2011. IEEE Trans. Magn. 47 (10), 3070–3073.
Uddin, R., Burger, R., Donolato, M., Fock, J., Creagh, M., Hansen, M.F., Boisen, A., 2016. Biosens. Bioelectron. 85, 351–357.
Vazquez, M., 2001. J. Magn. Magn. Mater. 226, 693–699.
Wang, T., Zhou, Y., Lei, C., Lei, J., Yang, Z., 2013a. Sens. Actuators B Chem. 186, 727–733.
Wang, T., Zhou, Y., Lei, C., Lei, J., Yang, Z., 2013b. Microchim. Acta 180 (13–14), 1211–1216.
Wang, T., Yang, Z., Lei, C., Lei, J., Zhou, Y., 2014a. J. Appl. Phys. 115 (22), 223901.
Wang, T., Yang, Z., Lei, C., Lei, J., Zhou, Y., 2014b. Phys. Status Solidi A 211 (6), 1389–1394.
Wang, T., Yang, Z., Lei, C., Lei, J., Zhou, Y., 2014c. Biosens. Bioelectron. 58, 338–344.
Wang, T., Guo, L., Lei, C., Zhou, Y., 2015b. RSC Adv. 5, 51330–51336.
Wang, T., Guo, L., Lei, C., Sun, X., Liu, Y., Zhou, Y., 2015a. Proceedings of the Institution of Mechanical Engineers, Part N: Journal of Nanoengineering and Nanosystems, 17403499155, 7, 3035,
Wheeler, H.A., 1942. Proc. IRE 30 (9), 412–424.
Yang, H., Chen, L., Lei, C., Zhang, J., Li, D., Zhou, Z., Bao, C.C., Hu, H., Chen, X., Cui, F., 2010. Appl. Phys. Lett. 97, 043702.
Yang, Z., Lei, C., Zhou, Y., Liu, Y., Sun, X.C., 2015a. Anal. Methods 7 (16), 6883–6889.
Yang, Z., Liu, Y., Lei, C., Sun, X.C., Zhou, Y., 2015b. Microchim. Acta 182, 2411–2417.
Yang, Z., Sun, X.C., Wang, T., Lei, C., Liu, Y., Zhou, Y., Lei, J., 2015c. Biomed. Micro. 17 (1), 1–8.
Yang, Z., Liu, Y., Lei, C., Sun, X.C., Zhou, Y., 2016. Microchim. Acta 183, 1831–1837.
Yavuz, C.T., Mayo, J.T., William, W.Y., Prakash, A., Falkner, J.C., Yean, S., Natelson, D., 2006. Science 314 (5801), 964–967.
Yuvchenko, A.A., Lepalovskii, V.N., Vas'kovskii, V.O., Safronov, A.P., Volchkov, S.O., Kurlyandskaya, G.V., 2014. Tech. Phys. 59 (2), 230–236.
Zhou, X.M., Xing, D., Zhu, D., 2008. Electrochem. Commun. 10, 564–567.